SANDIA REPORT
SAND2010-2289
Unlimited Release
Printed April 2010

Compressive Behavior of Fine Sand

Prepared by
Md. E. Kabir[1], Bo Song[2], Bradley E. Martin[3], and Wayne Chen[1]

1. School of Aeronautics and Astronautics, School of Materials Engineering, Purdue University, West Lafayette, Indiana
2. Sandia National Laboratories, California
3. Air Force Research Laboratory / Eglin, Florida

For
Vincent Luk,
Terminal Ballistics Technology Department, Sandia National Laboratories, New Mexico

Prepared by
Sandia National Laboratories
Albuquerque, New Mexico 87185 and Livermore, California 94550

Sandia National Laboratories is a multi-program laboratory operated by Sandia Corporation, a wholly owned subsidiary of Lockheed Martin Company, for the U.S. Department of Energy's National Nuclear Security Administration under contract DE-AC04-94AL85000.

Approved for public release; further dissemination unlimited.

Issued by Sandia National Laboratories, operated for the United States Department of Energy by Sandia Corporation.

NOTICE: This report was prepared as an account of work sponsored by an agency of the United States Government. Neither the United States Government, nor any agency thereof, nor any of their employees, nor any of their contractors, subcontractors, or their employees, make any warranty, express or implied, or assume any legal liability or responsibility for the accuracy, completeness, or usefulness of any information, apparatus, product, or process disclosed, or represent that its use would not infringe privately owned rights. Reference herein to any specific commercial product, process, or service by trade name, trademark, manufacturer, or otherwise, does not necessarily constitute or imply its endorsement, recommendation, or favoring by the United States Government, any agency thereof, or any of their contractors or subcontractors. The views and opinions expressed herein do not necessarily state or reflect those of the United States Government, any agency thereof, or any of their contractors.

Printed in the United States of America. This report has been reproduced directly from the best available copy.

Available to DOE and DOE contractors from
U.S. Department of Energy
Office of Scientific and Technical Information
P.O. Box 62
Oak Ridge, TN 37831

Telephone: (865) 576-8401
Facsimile: (865) 576-5728
E-Mail: reports@adonis.osti.gov
Online ordering: http://www.osti.gov/bridge

Available to the public from
U.S. Department of Commerce
National Technical Information Service
5285 Port Royal Rd.
Springfield, VA 22161

Telephone: (800) 553-6847
Facsimile: (703) 605-6900
E-Mail: orders@ntis.fedworld.gov
Online order: http://www.ntis.gov/help/ordermethods.asp?loc=7-4-0#online

SAND2010-2289
Unlimited Release
Printed April 2010

Compressive Behavior of Fine Sand

Md. E. Kabir[1], Bo Song[2], Bradley E. Martin[3], and Wayne Chen[1]

1. School of Aeronautics and Astronautics, School of Materials Engineering, Purdue University, West Lafayette, Indiana
2. Sandia National Laboratories, California
3. Air Force Research Laboratory / Eglin, Florida

Abstract

The compressive mechanical response of fine sand is experimentally investigated. The strain rate, initial density, stress state, and moisture level are systematically varied. A Kolsky bar was modified to obtain uniaxial and triaxial compressive response at high strain rates. A controlled loading pulse allows the specimen to acquire stress equilibrium and constant strain-rates. The results show that the compressive response of the fine sand is not sensitive to strain rate under the loading conditions in this study, but significantly dependent on the moisture content, initial density and lateral confinement. Partially saturated sand is more compliant than dry sand. Similar trends were reported in the quasi-static regime for experiments conducted at comparable specimen conditions. The sand becomes stiffer as initial density and/or confinement pressure increases. The sand particle size become smaller after hydrostatic pressure and further smaller after dynamic axial loading.

Keywords: Sand, triaxial mechanical behavior, Kolsky bar, pulse shaping, high strain-rate, moisture content.

ACKNOWLEDGMENTS

The Hopkinson bar experiments on fine sand documented in this report was funded by a research contract from Sandia National Laboratories (SNL), New Mexico to Purdue University. The research and development effort is a part of the Joint Munition Program (JMP), TCG-XI Terminal Ballistics Technology Project at SNL. The authors are indebted to Dr. Paul Butler, the JMP Manger at Sandia, for sponsoring this research effort, and to Dr. Vincent Luk, the TCG-XI Project Manager at SNL, for coordinating the Hopkinson bar experiments at Purdue University. They are also thankful to Mr. David Craft at SNL who provided important technical support in developing the experimental procedures.

CONTENTS

FIGURES

TABLES

This page intentionally left blank

NOMENCLATURE

A/D	analog to digital converter
ASTM	American Society for Testing and Materials
DC	direct current
DOE	Department of Energy
SNL	Sandia National Laboratories
JMP	Joint Munition Program
LVDT	Linear Variable Differential Transformer
MTS	Materials Testing System
PC	polycarbonate
SHPB	split-Hopkinson pressure bar
SNL	Sandia National Laboratories
SP	sand properties
USCS	Unified Soil Classification System

This page intentionally left blank

1. INTRODUCTION

Accurate predictions of intense transient events involving sand require quantitative description of the dynamic response of the sand materials. Besides the strain-rate effects, the effects of initial density, moisture level, and hydrostatic pressure need to be understood to effectively model the sand behavior under various loading and environmental conditions. Although sand is one of the most available materials in nature and in construction engineering, the dynamic response of this class of material has not been well understood. The quasi-static behavior of sand is extensively documented (e.g., Mitchell and Soga, 2005). There are attempts to develop unified constitutive models at these low loading rates (e.g., Pestana and Whittle, 1999; Pestana et al., 2002). Strain-rate effects have also been studied, but mostly within quasi-static range (e.g., Li et al., 2001). Dynamic response of sand has also been explored under vibration conditions (Li and Yang, 1998), drop-weight impact loading (Abrantes and Yamamuro, 2002), and using centrifuge modeling (e.g., Bruno and Randolph, 1999; Charlie et al., 2005). Material models for simulating stress waves from blast loading through soil are also proposed (Wang et al., 2004).

High-rate applications require the sand response to be characterized at high rates. However, geo-materials are not traditionally characterized under such loading conditions. Sand, for example, has been sporadically investigated to characterize the high-rate behavior over the past three or four decades. Charlie et al. (1990) tested 50/80 silica sand where most of the particle sizes are between the 50 and 80 mesh sizes (200 to 300 μm). The sand was unsaturated and subjected to dynamic compressive loading using a conventional Kolsky bar, also known as split-Hopkinson pressure bar (SHPB). The sand specimens were compacted using a steel hammer in four equal lifts and confined in a steel tube with steel wafers placed on both sides of the specimen. The primary focus was to evaluate the effects of saturation levels on the material longitudinal wave speed and transmission ratio (ratio of the transmitted stress to the incident stress).

Experiments conducted by Bragov et al. (1996) investigated plasticine and clay confined in a rigid steel jacket using a conventional Kolsky bar. Composite striker bars allowed both loading and unloading of the sample to be analyzed. These experiments characterized the mechanical properties in compression at a strain-rate of 4000 s^{-1}. Later work by Bragov (2008) investigated the dynamic response of dry sand using the same method. The dry sand was loaded at stress amplitudes of 80 MPa, 150 MPa, and 500 MPa. In these experiments, the specimens were passively confined with either aluminum or steel jackets allowing the specimen to be in a state of nearly uniaxial strain. Ross et al. (1986) used a conventional Kolsky bar to evaluate a single short pressure pulse traveling through long specimens of 20/40 dry sand, 50/80 dry sand, silica flour, clay, glass beads, and steel balls. The designation for the 20/40 dry sand is defined in the same manner as the 50/80 sand, but with a majority of the particle sizes between the 20 and 40 mesh sizes (425 to 850 μm).

Static and dynamic compaction methods were investigated in conjunction with varying moisture contents. Pierce (1989) evaluated moisture and confining effects using a conventional Kolsky bar for 20 and 30 Ottawa sand and Eglin sand. These materials have particles predominately between the 20 and 30 mesh sizes (600 to 850 μm). Tri-axial confining pressures were generated by applying axial pressure through the incident/transmission bars and pressurizing water between a thin membrane and the inner wall of the confining cell for lateral confinement. The data

collected included stress transmission ratios and longitudinal wave speed data for varying percent saturation levels at confining pressures of 0 KPa and 310 KPa. Felice et al. (1987a) evaluated clayey silty sand using a conventional Kolsky bar with specimens compacted to an initial density of 1.87 g/cm^3. The clayey silty sand was evaluated at strain-rates from 500 s^{-1} to 5000 s^{-1}, and was achieved using different specimen dimensions and striker bar velocities. The focus was to determine if the basic assumptions used in Kolsky bar techniques could be satisfied and if the data was repeatable.

Later work by Felice et al. (1987b) conducted 26 experiments to investigate the high strain-rate behavior of clayey sand with varying water contents, specimen dimensions, and loading stresses. Veyera (1994) studied the uniaxial stress-strain behavior of compacted moist Eglin sand, Tyndall sand, and 20-30 Ottawa sand at strain rates of 1000 s^{-1} and 2000 s^{-1} using a conventional Kolsky bar. The specimens had varying percent saturations from 0% to 100% with specimens at 20% saturation having a similar response as dry sand and percent saturations 40% and higher having a stiffer response than dry sand.

These previous research efforts have contributed to the understanding of the dynamic mechanical response of sand, primarily those of Veyera (1994), Felice et al. (1987a), Felice et al. (1987b), and Bragov (2008). These contributions form part of the basis for developing physics-based constitutive models under certain conditions. Some of these efforts either compact the sand specimens prior to testing or require additional experiments to fully characterize the dynamic behavior. The compaction of specimens has been shown to increase the stiffness of the samples while initiating lock-up much earlier in the material response. This compaction may also make results appear contradictory, for example, the results presented later in this report on uncompacted sand show opposite trends in moisture effects as compared to the results by Veyera (1994). Compaction of soils exists in the underlying layers of in situ soils, but no efforts have exclusively looked at uncompacted soil, which represents the surface layers of an in situ soil bed. Similarly, Felice et al. (1987b) compacted all specimens while testing clayey sand, which is a very different material, at various moisture contents of 7%, and 10% - 12% with two different aspect ratios. Bragov et al. (1996) and Bragov et al. (2008) investigated the dynamic response of plasticine, clay, and sand. Plasticine and clay materials are cohesive with higher degrees of saturation and typically have much higher densities than sand. Bragov (2008) also investigated the dynamic behavior of dry sand. The samples in earlier efforts by Ross et al. (1986), Charlie et al. (1990), and Pierce (1989) had larger aspect ratios, leaving the dynamic stress equilibrium during the early stages in the specimen in question due to the low longitudinal wave speed of sand.

Although the triaxial compression test is presently the most widely used procedure for determining the strength and stress-deformation properties of soils, the rate behavior is still largely missing in literature. A considerable research has been done to improve the triaxial experimental method and its applications (Henkel 1952; Gibson 1954; Bishop, 1962, 64 and Andersen 1960). More recently, Menzies et al. (1988) have developed microprocessor-controlled triaxial setup where the axial deformation and pore pressure were monitored. In the same year, Li et al. (1988) developed an automated triaxial testing system where the loading is controlled by a closed-loop feedback scheme capable of performing stress or strain controlled tests in the standard triaxial environment. Germaine and Ladd (1988) investigated the problems in the

testing equipment and procedures that causes errors in the measured properties of the specimens. They showed that some changes in the conventional triaxial testing practice can provide better estimates of in-situ soil behavior under field conditions. Peters (1988) described the difficulties posed by the low plasticity soils including silty and sandy clays, silts, and sands. The controlled variations in the differences in the principal stresses allow the exploration of the specimen response over wide ranges of stress paths and states. For example, Heard and Cline (1980) characterized the compressive response of polycrystalline ceramics under very high pressures. Dobry et al. (1982) investigated on the effect of the cyclic loading on the strain controlled triaxial tests of sands. They showed that the cyclic shear strain is the fundamental parameter governing undrained pore pressure builds up in saturated sand. More recently, Lee et al. (2004) performed triaxial experiments on SiC-N ceramics to determine the shear failure envelope under low pressures. The results indicate the pressure dependence of the failure strength of SiC-N ceramics. Macari and Hoyos, Jr. (2001) performed a series of triaxial tests on recompacted silty sand to study the stress-strain behavior of an unsaturated soil. The experiments were conducted in a stress/suction-controlled true triaxial setup controlling the major, intermediate and minor principal stresses. The results show a significant influence of matric suction (difference of pore air pressure from pore water pressure) on the size, position, and shape of the potential failure envelopes in the octahedral stress plane.

Triaxial testing under a variety of loading modes has been used to achieve various loading conditions. For example, stress path control is used in the study of path dependence of soil behavior (Bishop and Wesley, 1975; and Hsieh, 1985). Kitamura and Haruyama (1988) performed conventional triaxial drained compression tests on three kinds of soils: clayey soil, Toyoura sand, and soft sedimentary rock under wide ranging confining pressure. The conclusion is that the mechanical behaviors of these soils are similar under wide ranging confining pressure although these materials are often treated as different. Dennis (1988) performed undrained triaxial experiments on four different isotropically consolidated sand specimens. They found that both sample preparation techniques and method of loading affect the undrained steady state strength.

Despite these research efforts, the high-rate response of sand is still not well understood. This technology gap identifies the need for systematic research on the moisture and rate effects on sand response. Part of the reason why sand is not typically characterized dynamically is because of the complexity of the specimen material and the lack of standardization of the dynamic experimental methods. Due to the complex nature of the material, variations of the testing conditions inherent in the characterization methods need to be minimized in order to reveal the intrinsic material response. Recent developments in Kolsky bar techniques have significantly improved the ability to control the testing conditions the specimen experiences. For example, the conventional Kolsky bar generates a trapezoidal incident pulse with very fast initial loading rates. Such fast loading rates may be needed to accelerate a metallic specimen into high-rate flow. However, in the case of geologic materials the longitudinal wave speeds are slower, which requires slower loading rates to allow the specimen to acquire stress equilibrium and constant strain-rate.

In this research, the compressive response of fine sand is investigated, with the strain rates, specimen density, moisture level, and confining pressure systematically varied. A modified

Kolsky bar using a pulse shaping technique is used to generate controlled dynamic loading pulses that allow the specimen to deform uniformly at constant strain rate under dynamic equilibrium. The stress equilibrium conditions are checked in each dynamic experiment. Dynamic triaxial experiments are realized by integrating pressure vessels with the Kolsky bar. The pulse-shaping technique allows the systematic variation in strain rates in the specimens under Kolsky bar loading, with or without confinement. Corresponding experiments at quasi-static strain rates are also performed to study the rate effects over a much wider range. Experimental results show negligible strain-rate effects on the compressive response of the sand within the strain-rate range covered in this research. Higher initial density stiffens the compressive response significantly. Adding moisture softens the sand. The axial stiffness increases with increasing confining pressure. Such results contribute to creating a quality database of dynamic properties to be used for the development of physics-based constitutive models for sand. In the following sections the experimental technique is briefly described with results presented and discussed.

2. MATERIAL DESCRIPTION

The material studied in this research is silica based fine grain sand; klin dried and poorly graded (ASTM 2001). Figure 1 shows the sand particle size distribution provided by the manufacturer, which indicates that most sand particles are in the diameter range from 150 to 450 μm. The geometric sand properties are documented in Table 1.

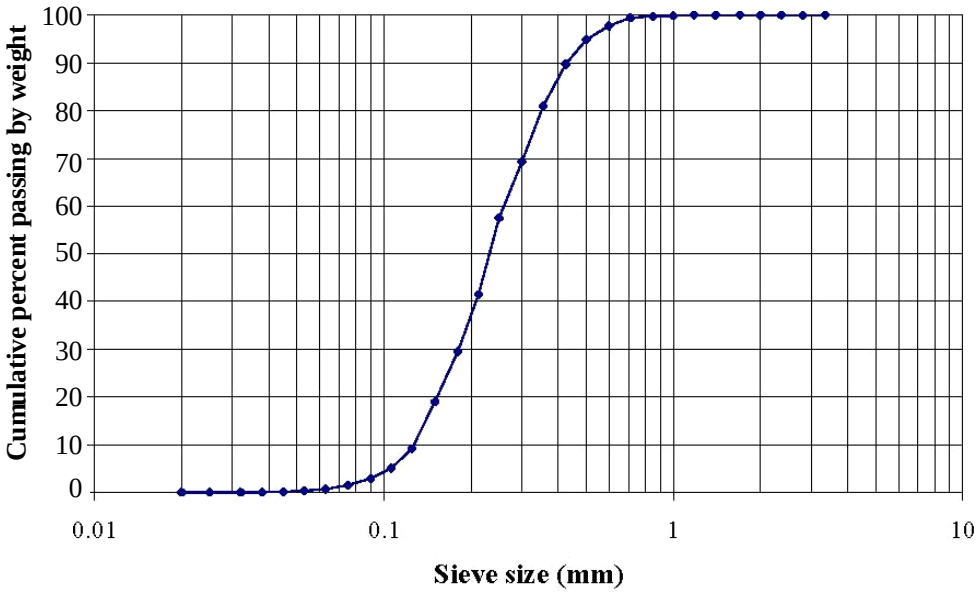

Figure 1. Quikrete #1961 particle size distribution

Table 1. Quickrete # 1961 Properties

USCS classification	*SP*
Specific gravity	2.72
D_{10} particle size (mm)	0.137
D_{30} particle size (mm)	0.211
D_{50} particle size (mm)	0.281
D_{60} particle size (mm)	0.32
[b] C_u	2.33
[c] C_c	1.02
[d] Percent passing # 100 sieve (%)	12.5
[d] Percent passing # 200 sieve (%)	2.7
Maximum dry density (kg/m^3)	1630
[a] Maximum dry density (kg/m^3)	1400
[b] Unified soil classification system [c] Coefficient of uniformity [d] Coefficient of curvature [e] ASTM D4253 ASTM D4254	

This page intentionally left blank

3. EXPERIMENTAL SETUP

3.1. Uniaxial Experimental Setup

Uniaxial experiments are performed under both dynamic and quasi-static loading conditions. The dynamic experiments are conducted using a modified Kolsky bar. The quasi-static tests are performed using an MTS servo-hydraulic experimental setup. The details of the setup and measurement techniques are briefly described below.

3.1.1. Dynamic Experimental Setup – Kolsky Bar

The modified Kolsky bar, also known as the split SHPB, which was used in this research for dynamic compressive experiments, is schematically shown in Figure 2. The conventional Kolsky bar was originally developed by Kolsky (1949) and consists of three elastic rods: a striker bar, an incident bar, and transmission bar. The striker bar is driven to apply an impact load on the specimen. To record the deformation and loading histories in the specimen, the incident and transmission bars are introduced as sensors and load carriers. The stress waves in the elastic bars carry information characterizing the loading conditions to the bar ends (Hopkinson, 1914). With the improvement in instrumentation for measuring stress waves and the increase in experience for conducting such instrumented experiments, the basic Kolsky bar setup has been continuously improved over the years (Lindholm, 1963; Follansbee, 1985; Nemat-Nasser, 1991; Gray, 2000). Besides the standard components in a conventional Kolsky bar, a pulse shaper at the impact end of the incident bar was employed in the modified Kolsky bar used in this research (Figure 2) to control the loading profile to allow sand specimens to deform at a nearly constant strain-rate under a nearly equilibrated stress state. The pulse-shaping technique was initially developed over three decades ago by Duffy et al. (1971) and then extensively used at Los Alamos National Laboratory (Follansbee et al., 1983). The technique was later quantitatively modeled (Nemat-Nasser et al., 1991; Frew et al., 2002 and 2005).

The specimen was sandwiched between the incident bar and the transmission bar. The impact of the striker, which is launched by the compressed air in the gas gun, on the end of the incident bar generates an elastic wave (incident wave), which propagates through the incident bar. The incident wave travels to the specimen and compresses it. Due to the mechanical impedance mismatch between the bars and the specimen, the incident wave is partly reflected back into the incident bar as a reflected wave and partly transmitted into the transmission bar as a transmitted wave. The incident and reflected waves are recorded by a strain gage (Vishay Micro-measurements; type: WK-13-125BZ-10C) mounted on the incident bar, and the transmitted wave is recorded by a strain gage on the transmission bar. A 28 volts DC power supply along with a half Wheatstone bridge (two strain gages on each bar) was employed to power the strain gages and measure the bar strains. The measured voltages were later converted into longitudinal bar strains and stresses. The recording device is typically a high-speed digital oscilloscope with pre-amplifiers or a computer with a high-speed A/D board. Figure 3 shows a photograph of the actual Kolsky bar setup for the sand experiments conducted in this research.

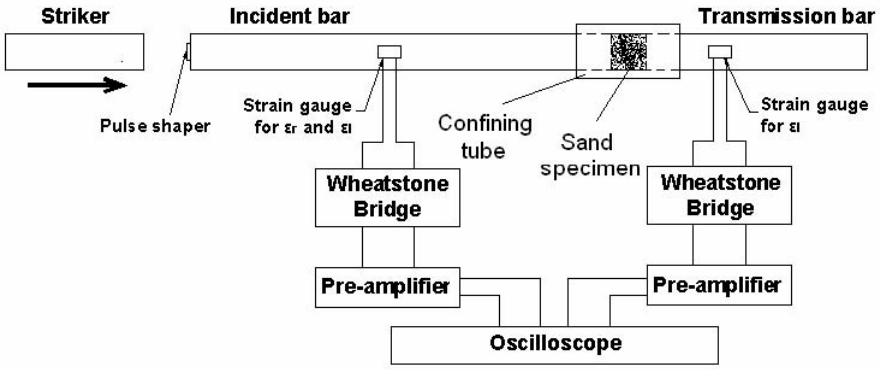

Figure 2. A schematic of the modified Kolsky bar system

Figure 3. A photograph of the actual Kolsky bar for dynamic sand experiments

During a Kolsky bar experiment, the pressure bars must remain elastic and their lengths should be long enough to avoid overlapping in the elastic waves, which are necessary for an accurate data reduction based on the 1-D elastic wave theory. In addition, the ends of the bars in contact with the specimen must remain flat and parallel throughout the dynamic loading, which is one of the necessary conditions for the specimen to deform under a uniaxial stress condition. Based on one dimensional wave analysis, the strain rate, strain, and stress histories in the specimen can be calculated from the recorded bar-surface strain signals with the following equations (Gray 1997, 2000).

$$\dot{\varepsilon}(t) = \frac{C_0}{L_s}\left[\varepsilon_i(t) - \varepsilon_r(t) - \varepsilon_t(t)\right] \qquad (1)$$

$$\varepsilon(t) = \frac{C_0}{L_s}\int_0^t [\varepsilon_i(t) - \varepsilon_r(t) - \varepsilon_t(t)]dt \qquad (2)$$

$$\sigma(t) = \frac{A_0}{2A_s} E_0 [\varepsilon_i(t) + \varepsilon_r(t) + \varepsilon_t(t)] \qquad (3)$$

where $\epsilon_i(t)$, $\epsilon_r(t)$ and $\epsilon_t(t)$ are incident, reflected, and transmitted strain histories, respectively; A_0 is the cross-sectional area of the bars; E_0 and C_0 are Young's modulus and elastic bar wave speed in the bar material, respectively; A_S and L_S are initial cross-sectional area and length of the specimen, respectively. For the sand experiments, the specimen diameter is the same as the bar diameter, $A_s = A_0$.

When the specimen is in a state of uniform stress (this poses the necessary condition for dynamic stress equilibrium),

$$\varepsilon_i(t) + \varepsilon_r(t) = \varepsilon_t(t) \qquad (4)$$

Equations (1)-(3) can be simplified as

$$\dot{\varepsilon}(t) = -2\frac{C_0}{L_s}\varepsilon_r(t) \qquad (5)$$

$$\varepsilon(t) = -2\frac{C_0}{L_s}\int_0^t \varepsilon_r(t)dt \qquad (6)$$

$$\sigma(t) = \frac{A_0}{A_s} E_0 \varepsilon_t(t) \qquad (7)$$

Therefore, once the incident, reflected and transmitted signals are measured, the stress-strain data for the material under investigation can be obtained if dynamic stress equilibration in the specimen is achieved. The equilibrium condition may not be satisfied automatically, especially when the specimen material is soft (Chen et al., 2002).

It has been found that it is impossible to achieve dynamic stress equilibrium in a conventional Kolsky bar experiment on soft materials (e.g., rubbers) due to the very high initial loading rate in the incident pulse even for very thin specimens (Chen et al., 2002). It is therefore necessary to modify the loading profile of the incident pulse. An efficient method to control the loading pulse is to use a pulse shaper at the impact end of the incident bar (Figure 2). The pulse shaper is commonly a small disk made of metal, plastic, rubber, or even paper. The selection of the pulse shapers is specimen material and strain-rate dependent, and will vary from experiment to experiment. Proper control of the incident pulse profile through varying material and dimensions of the pulse shaper, together with the variations in striker velocity, material and length, can achieve dynamic stress equilibrium and constant strain-rate deformation in a specimen. It is essential to collect accurate and reliable stress-strain data at various constant strain rates to investigate the strain-rate effects of materials and to develop strain-rate-dependent material models.

In this study, the bars in the modified Kolsky bar with pulse shaping technique had a common diameter of 19.05 mm. Two kinds of bar materials (steel and aluminum) were used to characterize the sand specimens under different confinement levels using polycarbonate (PC) tubes, polyolefin heat shrink tubes, and steel tubes. In particular, the steel bar was used when the sand specimens were confined with the PC and the steel tubes; whereas the aluminum bar was employed when the sand specimens were confined with the polyolefin heat shrink tubes.

3.1.2. Quasi-static Uniaxial Setup

Quasi-static compressive experiments of the sand were conducted with an MTS 810 materials test system in the mode of displacement control. The schematic of the testing section is shown in Figure 4. Two 19.05-mm-diameter steel bars are held and guided with an alignment frame to keep a precise alignment during compression. Besides the same specimen, the configuration in the MTS experiments is the same as in the Kolsky bar experiments such that the strain rate is the only variable from the quasi-static to dynamic experiments.

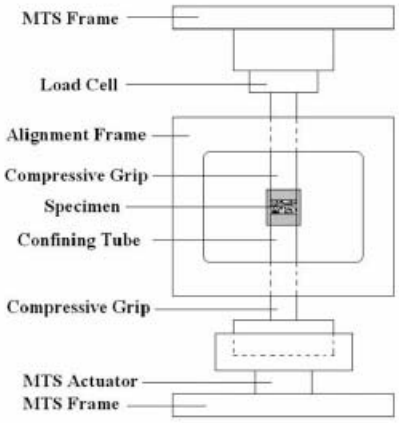

Figure 4. A schematic of gripping system in MTS810 for sand testing

For comparison between the compressive responses of moisture and dry sand, quasi-static uniaxial strain tests have been accepted as well controlled experiments with well defined boundary conditions. In this section, results of quasi-static uniaxial strain experiments for dry and partially saturated sand conducted with the same boundary conditions and material are qualitatively compared to the results in this investigation. A uniaxial strain test loads the specimen in the axial direction and constrains the specimen in the lateral direction with the radial loading and displacement recorded. The assembled specimen is shown in Figure 5 and Figure 6.

The specimen has three membranes placed around it with the outer membrane coated with liquid synthetic rubber to prohibit deterioration from the confining fluid (Williams et al., 2006). The specimen is mounted with a Linear Variable Differential Transformer (LVDT) (Figure 6) to measure the axial strain. A lateral deformeter is mounted at the specimen mid height to measure radial displacement. The lateral deformeter has a LVDT mounted to a hinged ring, so as the specimen is displaced radially, the ring opens measuring the displacement. The specimen is placed in a pressure vessel where a confining fluid is used to provide lateral confinement while

axial loading is provided by a servo controlled piston. Additional information on the execution and instrumentation used for the uniaxial strain experiments is reported by Williams et al., 2006.

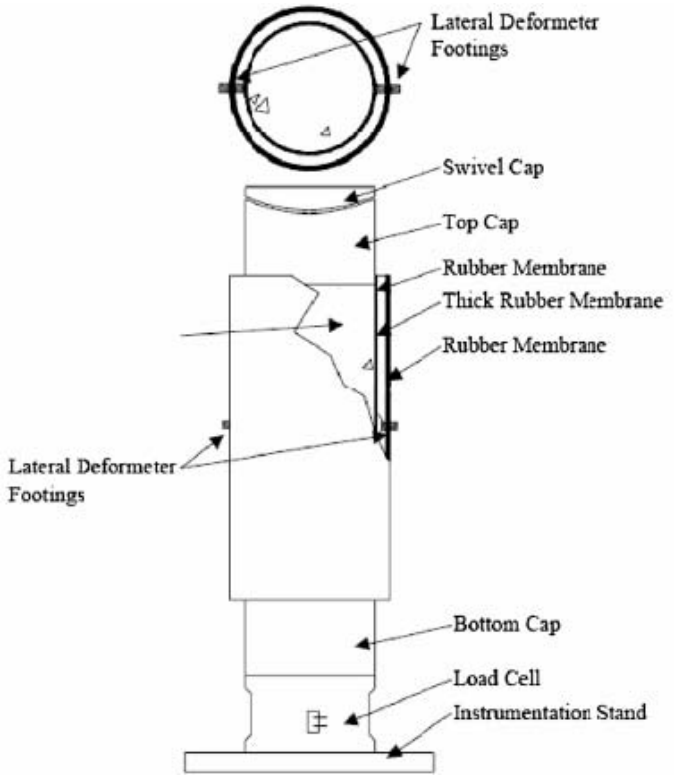

Figure 5. Schematic of triaxial strain specimen assembly (Williams et al., 2006)

Figure 6. Photograph of the triaxial specimen assembly with instrumentation (Williams et al., 2006)

3.1.3 Dynamic Triaxial Setup

For the dynamic triaxial experiment, we used a modified Kolsky bar. The modification was implemented using the apparatus schematically shown in Figure 7. Two pressure chambers were integrated (one around the sample, termed as radial chamber and the other at the opposite end of the transmission bar, termed as longitudinal chamber) with the Kolsky bar. The specimen is sandwiched in between the incident and transmission bars. To offset the hydrostatic compression in the pressure bars during the hydrostatic pressure state of the experiments, tensile tie-rods were installed symmetrically around the pressure bars in the center. Figure 8 shows a photograph of the actual dynamic triaxial setup for the sand experiments conducted in this research.

The basic relations between the parameters in a conventional triaxial experiment are described in the Appendix 1. Dynamic triaxial experiments are performed in two stages. In the first phase hydrostatic pressure is applied using a high pressure fluid (kerosene and motor oil in a 4:1 ratio). In the second phase, dynamic load is applied by impacting the striker on the incident bar. A pulse shaper at the impact end of the incident bar is also employed to control the loading profile to allow sand specimens to deform at a nearly constant strain rate under a nearly equilibrated stress state. The details of the measurement techniques are described below.

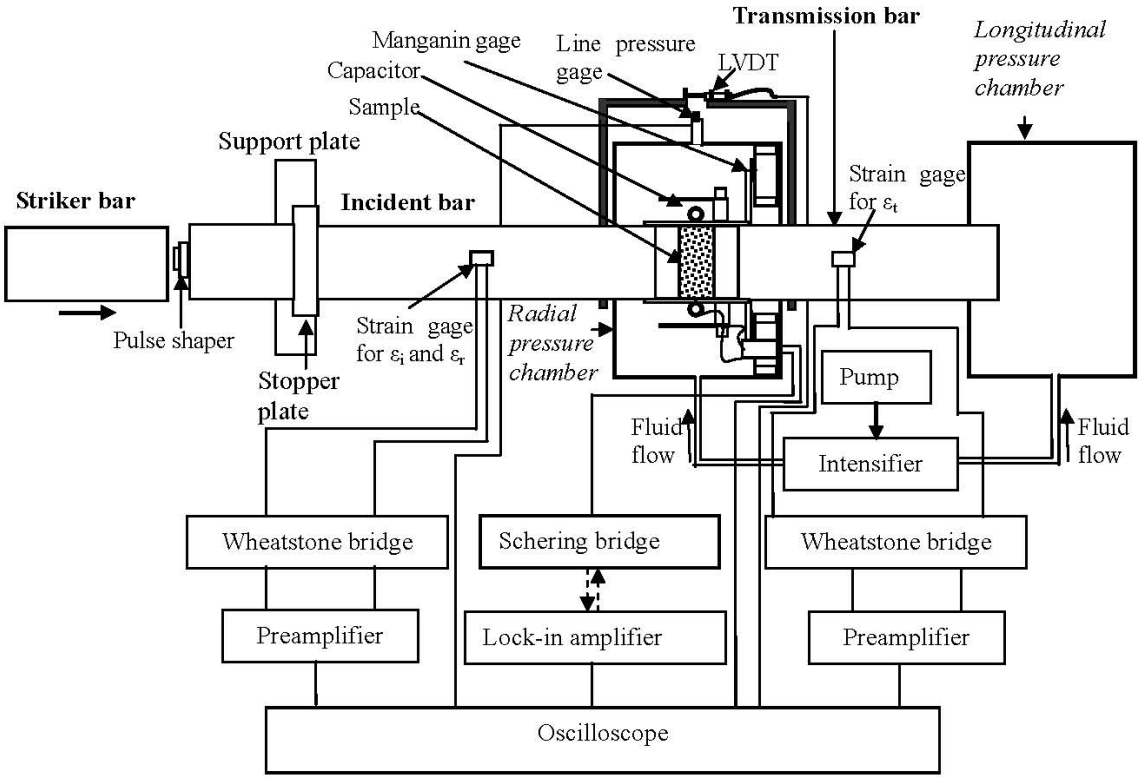

Figure 7. A schematic of the dynamic triaxial test system

Figure 8. Photograph of the actual dynamic triaxial setup for sand experiments

Axial Stress and Axial Strain

The axial stress and axial strain of the sand specimen in the hydrostatic compression phase were measured by the line pressure gage (Honeywell Sensotec; model: HP, range: 75000 psi) and the Linear Variable Differential Transformer (LVDT from Honeywell; type: M-5C). Both of these provide readouts in terms of voltage which are later converted into pressure and deformation by multiplying with the calibration factors given in Appendix 2. To mount the LVDT, two supports ware placed on the incident and transmission bar around the radial confinement chamber, as shown in Figure 9. The lead and core of the LVDT are mounted on top of those supports. As the incident bar is restricted to move at the impact end, the pressure in the longitudinal confinement chamber pushes the sand specimen to deform longitudinally. During hydrostatic pressure phase, the bars also deform. The bar deformation between the LVDT supports is a part of the deformation the LVDT measures. This bar deformation is subtracted to obtain the true deformation on the specimen. For measuring the bar deformation, the supports were placed at the same distance on the bars and both the bars are butted together in the middle chamber with a heat shrink tube.

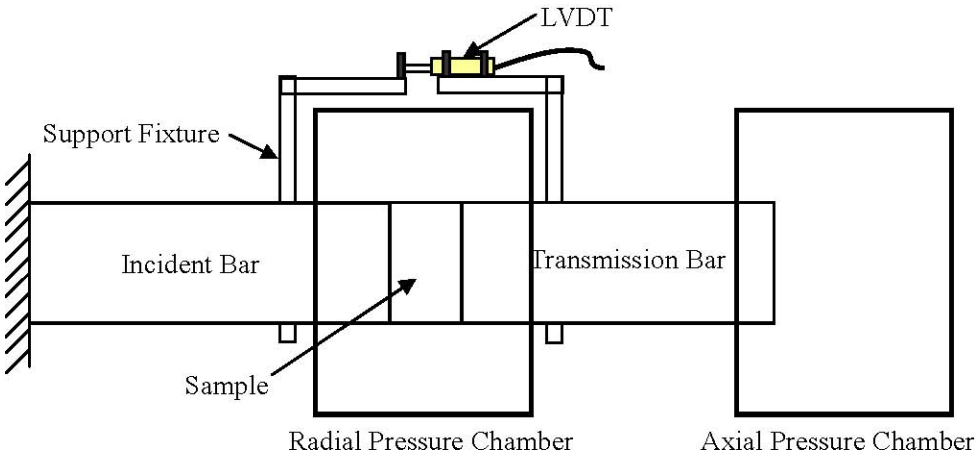

Figure 9. Scaffolding arrangements for hydrostatic length change measurement

The axial strain in hydrostatic phase, ε_{ah} is computed by diving the measured axial deformation, Δl (change in sample length from LVDT) by the original sample length, l_o, i.e. $\varepsilon_{ah} = \Delta l / l_o$. At the end of this phase the LVDT arrangement is dissembled as this cannot provide accurate dynamic length change reading but may interfere with dynamic loading process.

The stress and strain in dynamic part of the experiment are measured from the strain gages placed on the incident and transmission bars as described in the dynamic uniaxial experimental setup.

Radial Stress and Radial Strain

The radial stress during hydrostatic phase is measured from the line pressure gage. During the dynamic phase, the additional dynamic pressure is measured by a manganin gage inside the pressure chamber. The manganin pressure gage is Vishay micro-measurements; type: LM-SS125CH-048. The calibration of this pressure gage can be found in the Appendix 2.

The radial strain under both hydrostatic pressure and dynamic loading is measured by the capacitor assembly shown in

Figure 10. A capacitor arrangement was made inside the radial chamber with a spring on the sample and a small copper tube placed on the transmission bar end. The diameter of the copper tube is chosen such that the spring does not touch the copper tube during the maximum deformation of the sample in the dynamic loading phase. The length of the copper tube is much bigger than the spring diameter, so that most of the electrical fringes can be covered inside the copper tube.

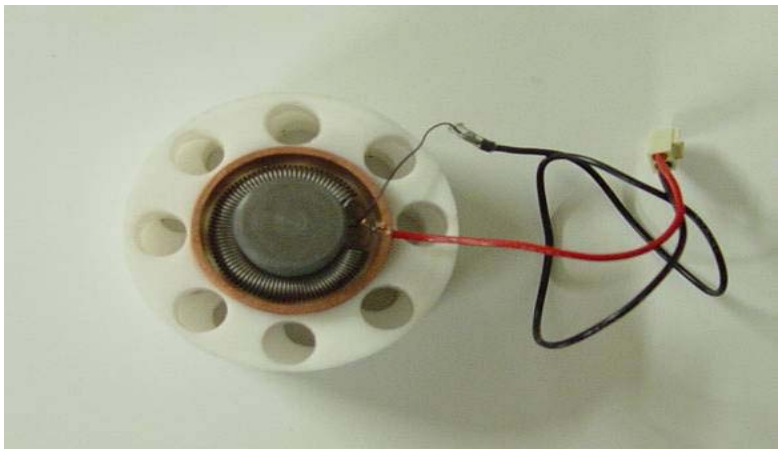

Figure 10. Design of a capacitor for the diameter measurement

During experiments when the sample deforms in radial directions, the spring moves with the outer surface of the sample. But the outer copper tube remains at the same location. This makes a relative change in distance between the copper tube and the spring; thereby producing a capacitance change. We employ a Schering Bridge, as shown in Figure 11, for detecting the null point. With the use of a lock-in amplifier (Model DSP 7265) a precision AC signal (4V rms, 250 KHz) is generated which is an input to the Schering Bridge. The lock-in amplifier is also used as the null detector for the bridge circuit. The output of the lock-in amplifier goes through an

isolation transformer (G500TAM, Tamura) so that the ground connection can be taken out from the circuit. The stray capacitance is minimized by employing a Wagner-Earth voltage divider (Pilla et. al., 1999; Bera and Chattopadhyay, 2003). The lead-wire capacitance is minimized by using thin wires. The entire experimental setup is also connected to a common ground so that no electrical voltage variation can occur during the experiments. The change in the diameter during the experiment then makes the voltage change in the readout. This is then calibrated to give the diameter change accordingly. The calibration of the diameter-measurement system can be found in Appendix 2.

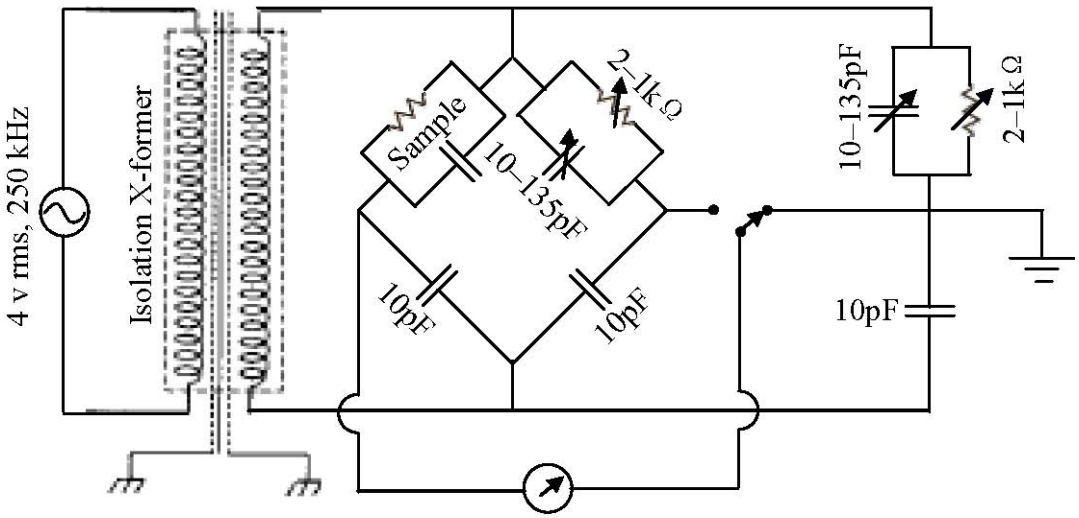

Figure 11. Schering Bridge design for the diameter change measurement

The radial strain, ε_r is computed by dividing the measured radial deformation, Δd (change in sample diameter from capacitor assembly) by the sample diameter, d, i.e. $\varepsilon_r = \Delta d/d$. For hydrostatic phase the original sample diameter, d_o and for dynamic phase the diameter after the hydrostatic phase d_{do} are used as sample diameter, d, for the two loading phases, respectively.

The readings from the line pressure gage, LVDT, and capacitance change during the hydrostatic pressure phase are recorded by a computer via LabVIEW 8.2 through a lock-in amplifier. The readings from strain gages, capacitance change, and the manganin gage during dynamic phase are recorded by a high-speed, four channel digital oscilloscope (Tektronix; Model: TDS3014C).

This page intentionally left blank

4 SPECIMEN THICKNESS DETERMINATION

Before the dynamic properties of sand are characterized, preliminary experiments were conducted to explore different testing configurations. In a valid Kolsky bar experiment, the specimen must be compressed uniformly. A necessary condition for uniform deformation is that the specimen must be in a state of stress equilibrium during the experiment. Besides the loading rate, specimen length has been demonstrated to be very critical to achieve stress equilibrium. A Cordin 550 high speed digital camera was used to monitor the high speed deformation of the sand specimen confined in a PC tube. The sand specimen had a density of 1.60 g/cc and the length varies from 28.4 mm to 13.1 mm. No pulse shaper was used in the specimen-length study. The sand specimens were made up by layers with natural brown and painted black colors such that the specimen appears stripped from the side view to reveal uniformity in axial deformation during axial loading.

Figure 12 through Figure 15 show the images of high-speed deformation, which were taken with the Cordin 550 at the frame rate of ~80,000 frames per second, of the sand specimens with the thickness of 28.4, 25.4, 15.2, and 13.1 mm, respectively. It is seen that the nearly uniform deformation was achieved better in the short specimens, with the thickness of 13.1 mm than in the long ones with the thickness of 28.4 mm. The 28.4-mm-long sand specimen was compacted initially from one end and then this compaction propagated towards the other end, as shown in Figure 12. Figure 12 through Figure 15 show how the specimen deforms more uniformly with decreasing specimen length. When the specimen length decreased to 13.1 mm, the specimen was deformed nearly uniformly, as shown in Figure 15. Figure 16 shows the corresponding stress histories to the frames in Figure 15. The frames in Figure 15 also show that the PC tube underwent an observable lateral expansion, indicating that the sand specimen was in neither one-dimensional stress nor one-dimensional strain states with the PC confinement. Further studies are necessary to determine the effects of confinement on the compression response of sand specimens. In this project, a polyolefin heat shrink tube and a 4340 steel tube were also used to provide a lower and an upper bound to the confinement on sand specimens.

Since the preliminary test data clearly indicates that a better uniformity of deformation and stress equilibrium can be achieved with shorter sand specimens, even shorter (9.3-mm-long) sand specimens were used for dynamic experiments where the specimen initial density was lower. Even though the specimen seemed to deform uniformly in the conventional Kolsky bar experiment, the strain-rate in the deformation process was not constant in the experiment. Therefore, the pulse shaping technique was employed in the sand experiments to facilitate constant strain-rates and a more uniform deformation during the early stages of the impact loading.

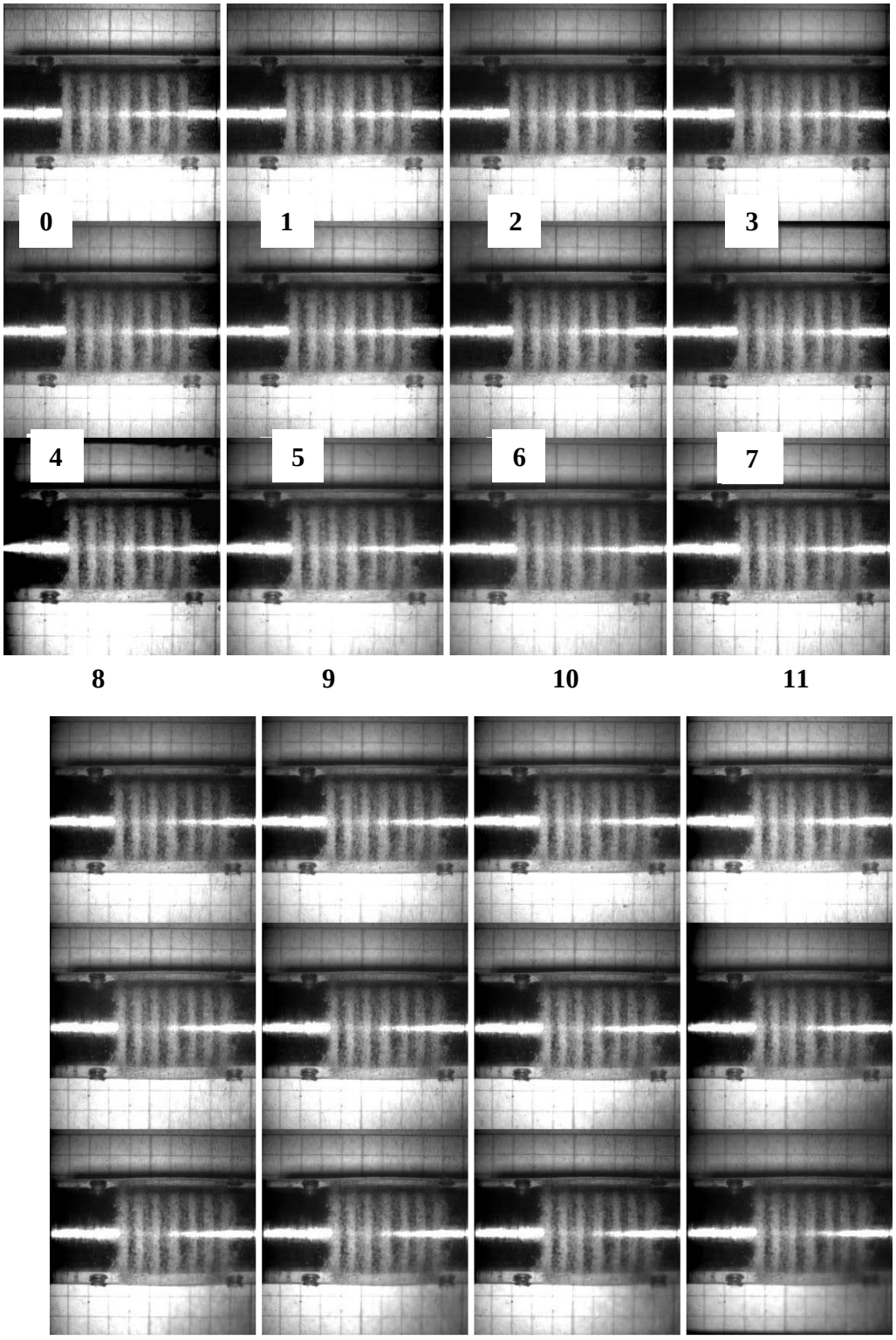

Figure 12. High speed deformation of a 28.4-mm-long dry sand specimen (Time interval: 12.3 microseconds)

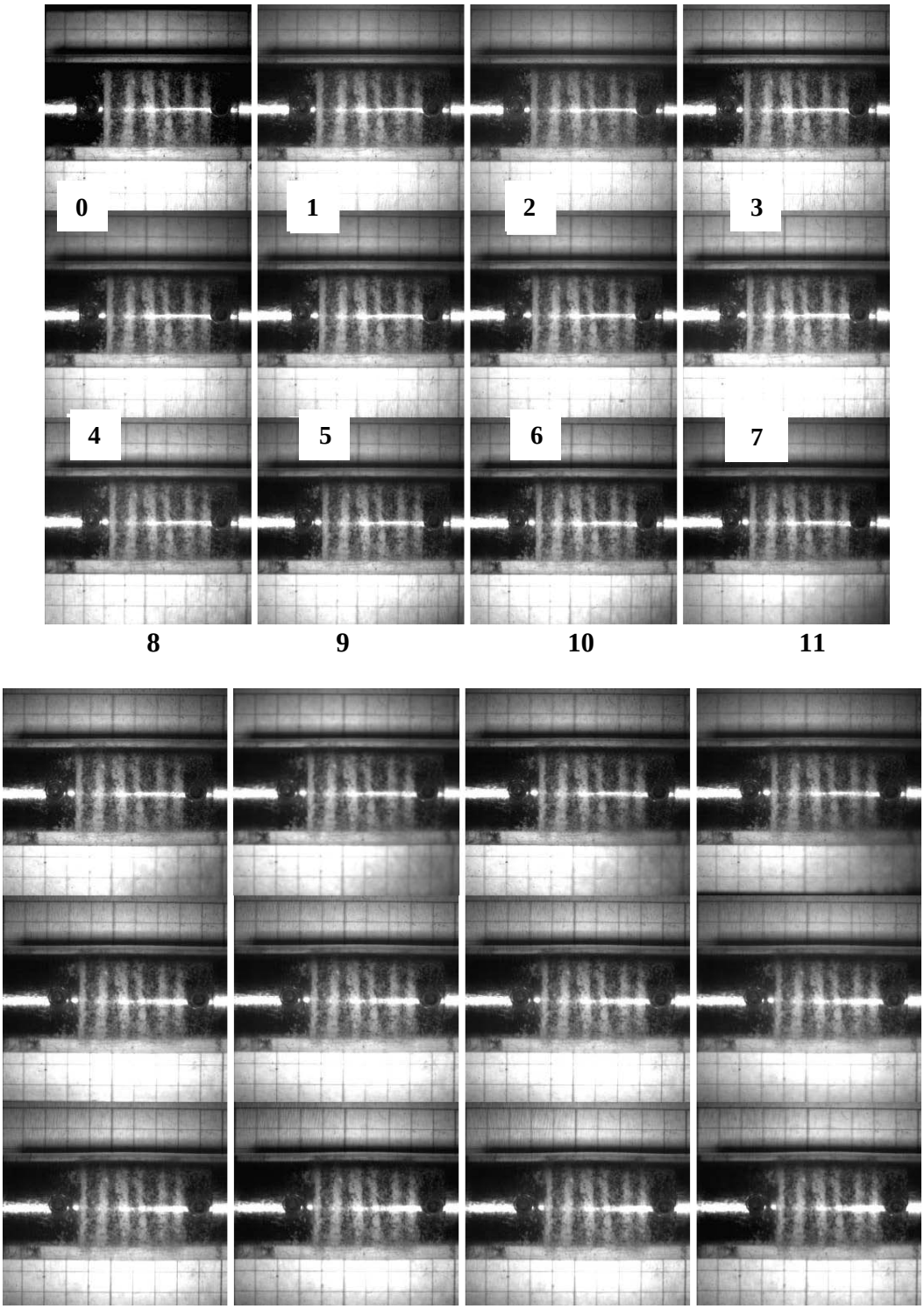

Figure 13. High speed deformation of a 25.4-mm-long dry sand specimen (Time interval: 12.4 microseconds)

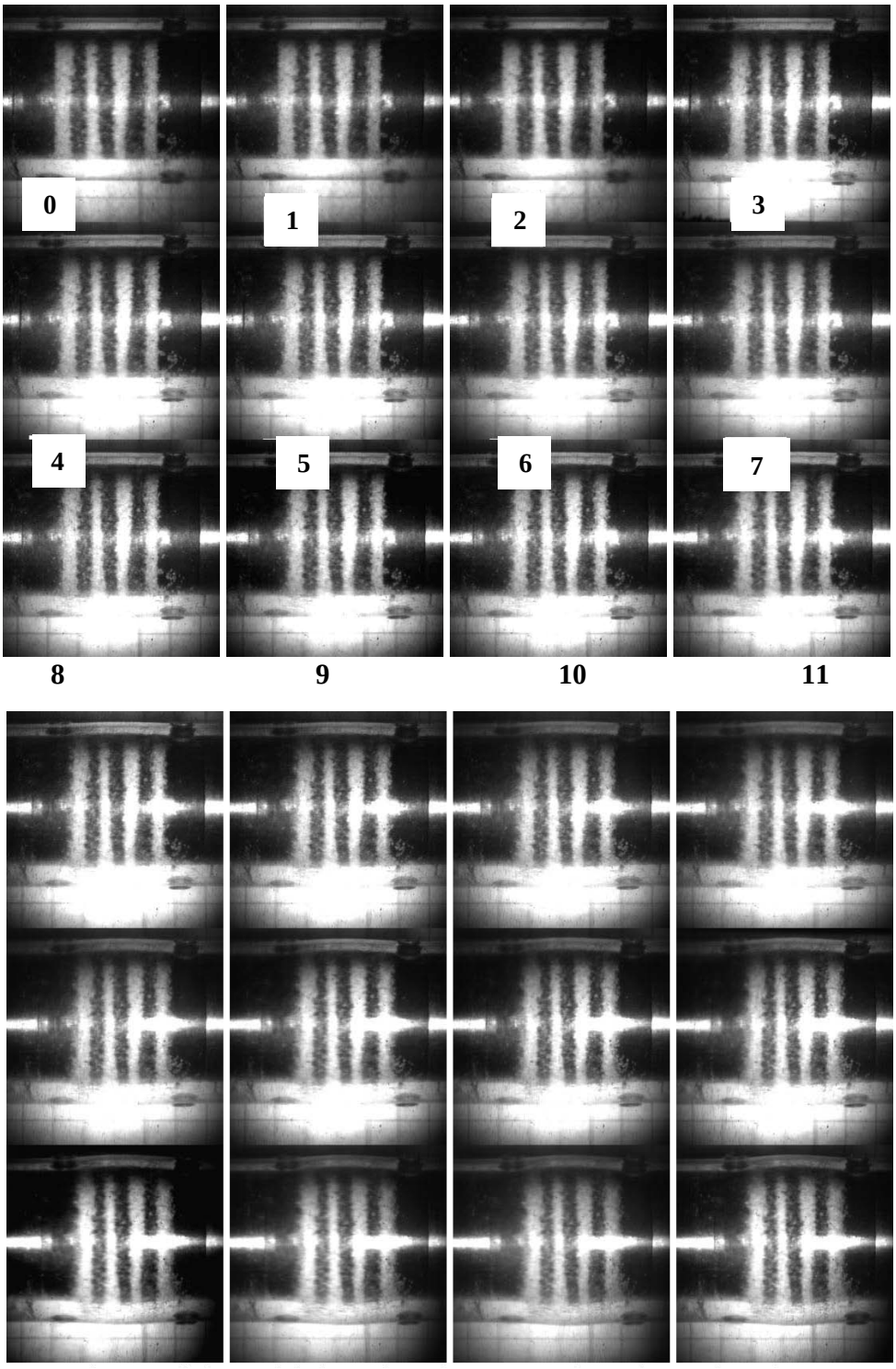

Figure 14. High speed deformation of a 15.2-mm-long dry sand specimen (Time interval: 12.4 microseconds)

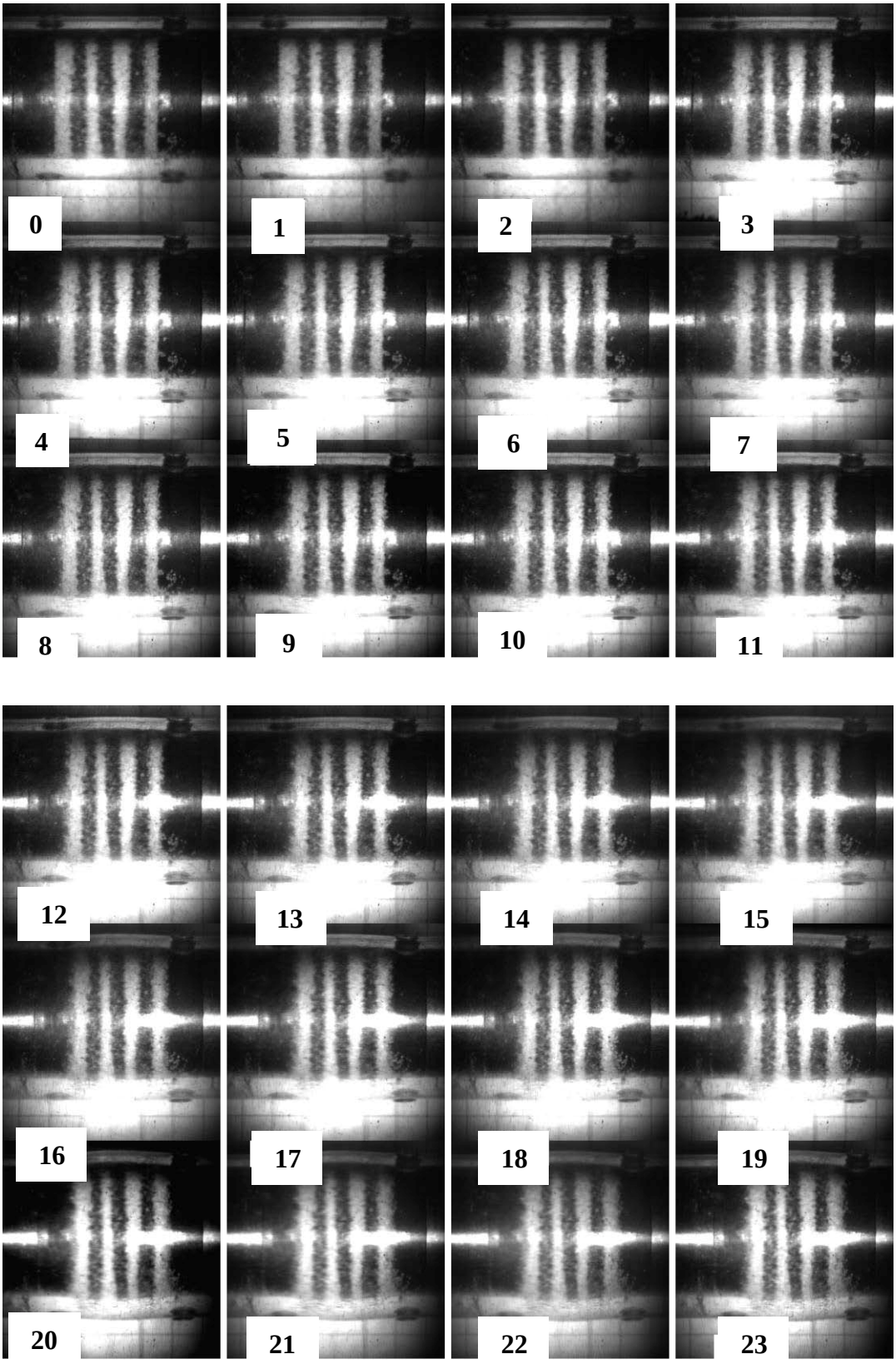

Figure 15. High speed deformation of a 13.1-mm-long dry sand specimen (Time interval: 12.6 microseconds)

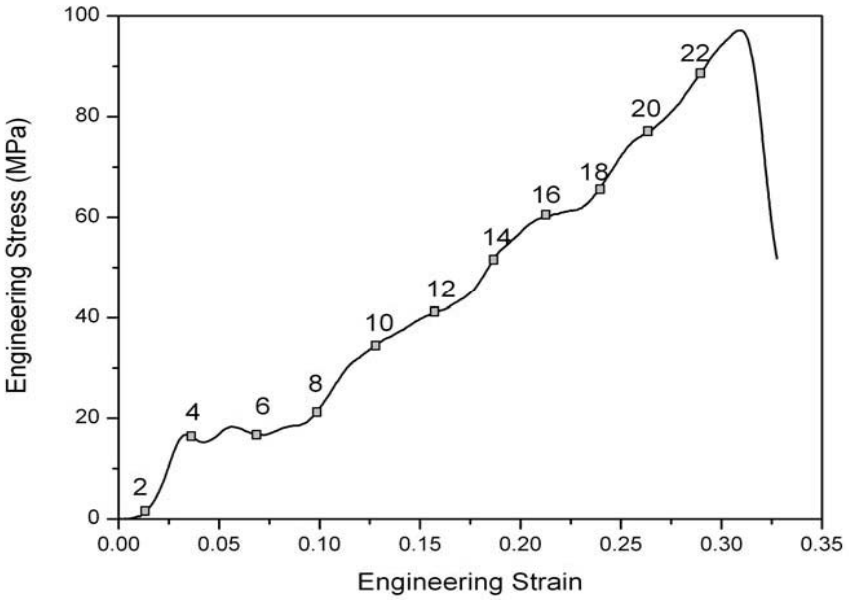

Figure 16. Engineering stress-strain curve from a 13.1-mm-long dry sand specimen

5. SPECIMEN PREPARATION

5.1 Uniaxial Experiments

The dry sand specimen was contained within three different types of tubes: polycarbonate, polyolefin heat-shrinking and steel tubes.

5.1.1 Contained with a Polycarbonate (PC) Tube (Figure 17)

The PC tube was commercially purchased from www.mcmaster.com and had an outer diameter of 25.4 mm and an inner diameter of 19.10 mm. Each PC tube was cut to down approximately 50-mm long for dynamic testing. The sand specimen preparation procedure is described below. First, a pair of small holes was drilled on the opposite sides of the tube. A 6.35-mm-thick, 19.05-mm-diameter steel platen was then placed inside the PC tube. The tube was fitted into the Kolsky bar by placing the incident and transmission bars inside the tube from the two open ends. One bar was held stationary while the other was moved towards it to align the incident bar, steel platen, and transmission bar along the loading axis. The PC tube was then moved back and forth to align the position of the holes to the steel platen. Two small set screws were installed into the holes to hold the platen at the hole position inside the tube. The tube with the platen position fixed was then removed from the Kolsky bar and placed vertically on the top of a 19.05-mm-diamter short rod. Dry sand (4.0 grams) was poured into the tube, which was then tapped slightly to make the top surface even. Another steel platen was placed on the top surface of sand, which was then slightly pressed with a smaller rod to make the specimen length at 9.30 mm (with a 1.50-g/cc density). It should be noted that, when the dry sand specimens were prepared at a higher density (1.62 g/cc), they were pre-compressed to 8.60 mm. In preparing the wet sand specimens, the 4.0-g sand was mixed with 7% (0.28 ml) water by weight. The assembled tube specimen was then installed in the Kolsky bar setup. At this step, the tube was turned horizontal with the top platen carefully held by fingers or set screws. A drop of super glue was placed on the end of the incident bar to hold the top platen in place when a tensile reflected wave arrived. Both the incident and transmission bars were moved into the tube from its two ends. At this point, the specimen thickness was checked again before the set screws were removed for the impact loading.

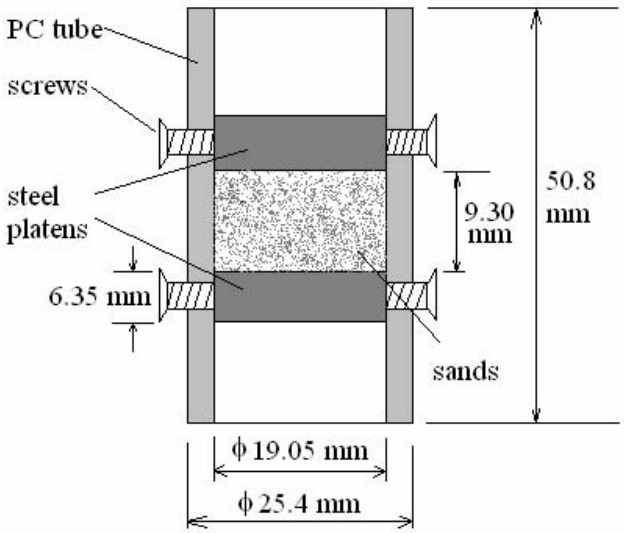

Figure 17. Schematic of sand specimen confined in PC tube

5.1.2 Contained with a Polyolefin Heat Shrink Tube (Figure 18)

The polyolefin heat shrink tube was commercially purchased from www.mcmaster.com and had an actual inner diameter of ~20.6 mm and a wall thickness of 0.3 mm. Each tube was cut to 52-mm long (Figure 18). The tube section was slid outside a 19.05-mm-diameter supporting rod that was marked at the position of 15 mm from the top end. A hair dryer was used to heat the tube until the tube is shrunk to snug-fit the rod. The shrunk tube was then moved to align the bottom edge of the shrunk tube at the marked line on the supporting rod. Since aluminum bars were used to compress the sand confined with the heat shrink tube, a 6.35-mm-thick, 19.05-m diameter aluminum platen was placed inside the shrunk tube. Dry sand (4.0-g) was poured into the tube, which was slightly tapped to make the top sand surface even. Another aluminum platen was placed on top of the sand specimen. Another rod was used to slightly press the aluminum platen until the top edge of the shrunk tube is at the position of 15 mm above the platen on the sand top surface. Therefore, the specimen length is $52.0 - 15.0 \times 2 - 6.35 \times 2 = 9.3$ mm (with 1.50 g/cc density). Two lines were marked at the positions of 15 mm from the end on the incident and transmission bars, respectively. The tube specimen was then moved from the supporting rods to the Hopkinson bar carefully. A drop of super glue was placed on the end of the incident bar before moving both incident and transmission bars into the tube from the two open ends. The specimen thickness was checked through verification of alignments between the edges of the shrunk tube and the marked lines on the incident and transmission bars.

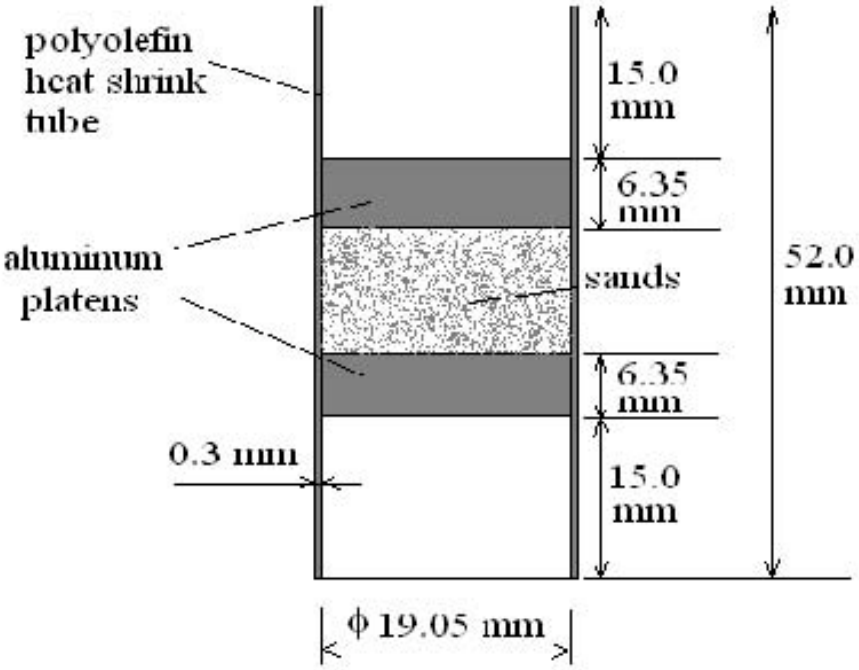

Figure 18. Schematic of sand specimen confined in polyolefin heat shrink tube

5.1.3 Contained with a 4340 Steel Tube (Figure 19)

The 4340 steel tube had an outer diameter of 25.4 mm, an inner diameter of 19.05 mm and 50.8-mm long. Two screwed holes were tapped on the opposite sides at the position of 14 mm from one end. The tube was slid on to a 19.05-mm-diameter supporting rod that was marked at the position of 14 mm from the top end. A 6.35-mm-thick, 19.05-mm-diameter steel platen was placed inside the tube. The steel platen was positioned by two set screws through both screwed holes such that the bottom edge of the steel tube aligns with the marked line on the supporting rod when the top of the rod was in contact with the platen. Dry sand (4.0-g) was poured into the tube, which was slightly tapped to make the top surface even. Another steel platen was placed on the surface of the sand. The steel platen was slightly pressed with another rod until the top edge of the steel tube was at the position, 14.8 mm from the bottom of the rod. Therefore, the specimen length was $50.8 - 14.0 - 14.8 - 6.35 \times 2 = 9.3$ mm (with a 1.50 g/cc density). Two lines were marked at the positions of 14 and 14.8 mm from the end on the incident and transmission bars, respectively. The tube specimen was then installed on the Kolsky bar. A drop of super glue was placed on the end of the incident bar before moving both incident and transmission bars into the tube from the two open ends, respectively. The specimen thickness was checked through verification of alignments between the edges of the steel tube and the marked lines on the incident and transmission bars.

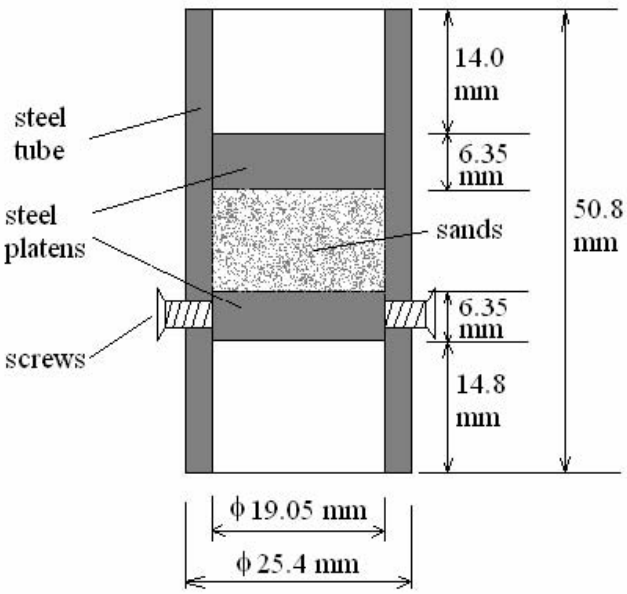

Figure 19. Schematic of sand specimen confined in steel tube

The dynamic compressive response of the sand was investigated in this study at various moisture contents ranging from 3% to 20% by weight with all specimens having the same dry density of 1.50 g/cm^3. All specimens were in an undrained condition, where water or air is not allowed to escape. The specimens were confined using a hardened 4340 steel tube with an outer diameter of 25.4 mm, inner diameter of 19.1 mm and length of 50.8 mm. The steel tube was used to replicate a simple uniaxial strain condition.

In sample preparation, after the dry sand was poured into the steel tube and tapped lightly to even the top surface, a 1-ml syringe was used to add the appropriate weight percent (e.g., 0.28 ml for 7% moisture by weight) of water to the sand. The water was slowly released from the syringe into the dry sand and evenly distributed over the top of the sand. The dry sand and water were then mixed mechanically and thoroughly. The second steel platen was then placed on top of the partially saturated sand and slightly pressed to ensure the interface between the platen and partially saturated sand is flat.

5.2 Triaxial Experiments

Figure 20 shows the sample preparation steps for the triaxial experiment. The sample preparation for the triaxial experiment is very similar to the polyolefin heat shrink tube confinement (section 5.1.2). A drop of super glue was placed on both the end of the incident bar and transmission bar before moving these bars into the tube from the two open ends. A heat gun was then used to heat the heat shrink tube and fuse it on to the bars. A piece of wet cloth was wrapped around the sample during the heating. This will reduce the chance to over heat the heat shrink tube in the test section. The specimen thickness was checked through verification of alignments between the edges of the shrunk tube and the marked lines on the incident and transmission bars.

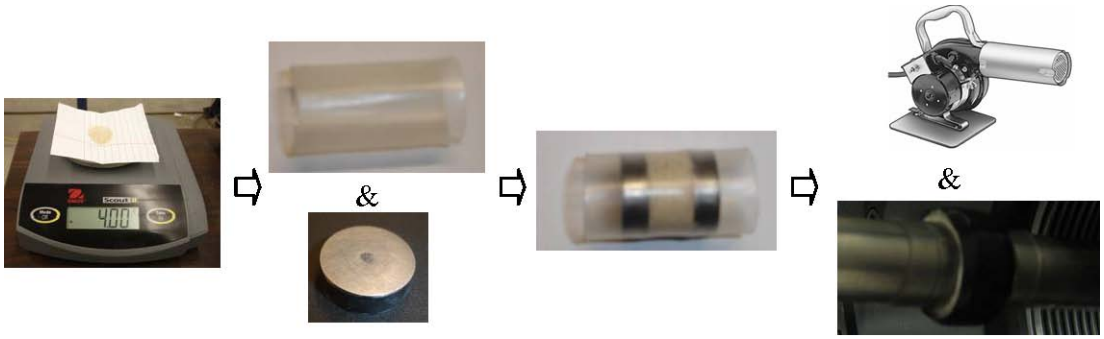

Figure 20. Schematic of the sample preparation steps for the triaxial experiments: a) **weighing 4 g of sand, b) heat shrinking the tube to the desired diameter; cleaning the platens, c) placing the sand inside the tube; and d) heating the tube to fuse on to the bar while covering the gage section.**

To check the fluid-sealing capacity by this specimen-installation process, we ran several experiments in the hydrostatic-pressure phase by increasing the hydrostatic pressure on the sample up to 150 MPa and then releasing it. The samples were then taken out of the seal for inspection. We found that the samples were leak free. As for an example, Figure 21 shows the sand condition before and after 150 MPa hydrostatic confinements. We also took out the sand after each experiment (including dynamic phase) and collected them for size distribution, which will be discussed later.

Figure 21. Sample leak check: a) Before applying pressure, and b) After applying 150 MPa confinement pressure

This page intentionally left blank

6. EXPERIMENTAL RESULTS

6.1 Uniaxial Experiment Results

6.1.1 Dynamic Uniaxial Results

The specimens confined with the PC tubes have a common dimension of 19.05 mm in diameter and 9.3 mm in thickness. The dry sand has a density of 1.50 g/cc. Figure 22 shows a typical set of oscilloscope records of incident, reflected, and transmitted pulses. The shape of the incident pulse in Figure 22 is different from that obtained in a conventional Kolsky bar experiment because of the application of the pulse shaping technique. When the material and dimension of the pulse shaper are appropriately selected, the profile of the incident pulse is controlled to ensure that the specimen deforms at a nearly constant strain rate under dynamic stress equilibrium. The dynamic stress equilibrium can be checked by a "2-wave" and "1-wave" method (Eq. (4), Gray, 1997, 2000). The left term in Eq. (4) represents the incident bar strain at the interface of the incident bar and the specimen, whereas the right term indicates the transmission bar strain at the interface of the specimen and the transmission bar. Figure 23 shows the dynamic stress equilibrium process in the specimen. The nearly overlapped stress histories at both ends of the specimen demonstrate clearly that the stress in the specimen was uniform.

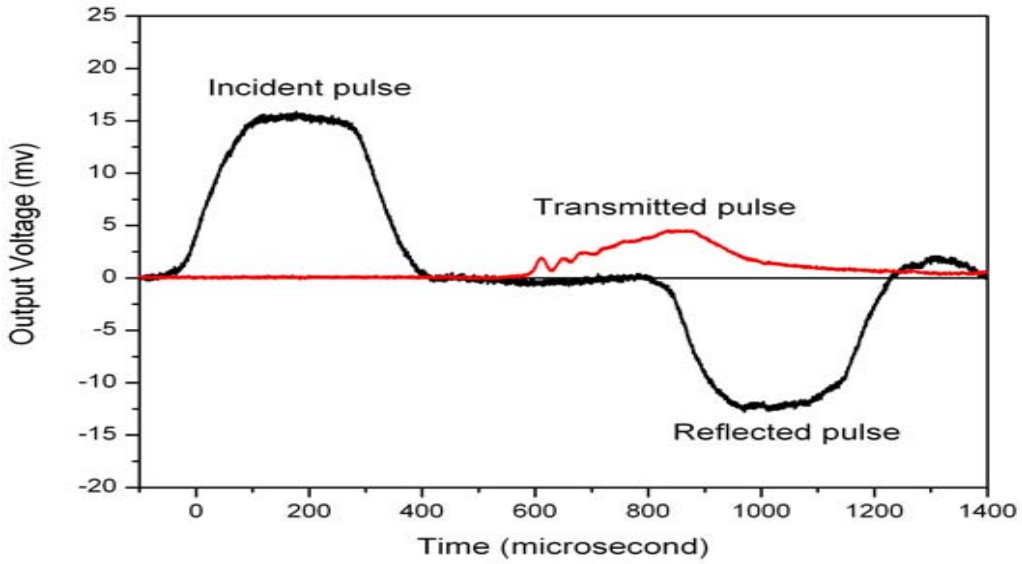

Figure 22. A typical set of incident, reflected, and transmitted pulses for dynamic uniaxial experiment

Under the dynamic stress equilibrium, the reflected pulse represents the strain-rate history in the specimen (Eq. (5)). Figure 24 shows the strain-rate and strain histories in the specimen. The strain rate is nearly constant (470/s) from ~150 to 325 μs corresponding to the strains from 3% to 11%. Therefore, the specimen was deformed uniformly under dynamic stress equilibrium over most of the loading duration, indicating that the resultant stress-strain curve in Figure 25 is valid and accurate. The specimen exhibits a nearly linear compressive behavior when the strain is smaller than 11%.

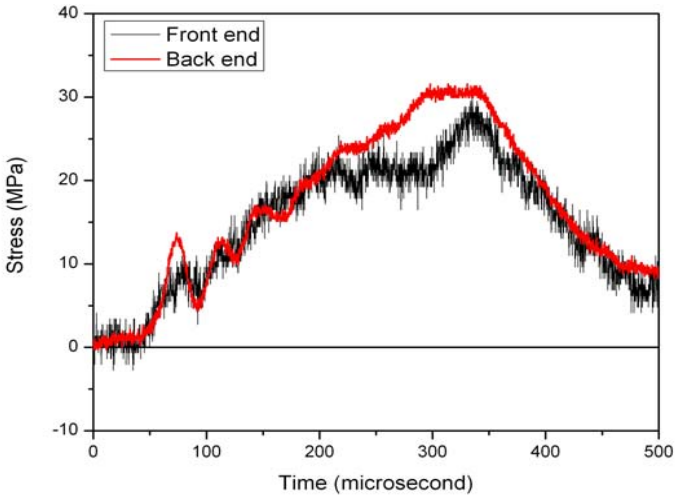

Figure 23. Dynamic stress equilibrium process for uniaxial experiment

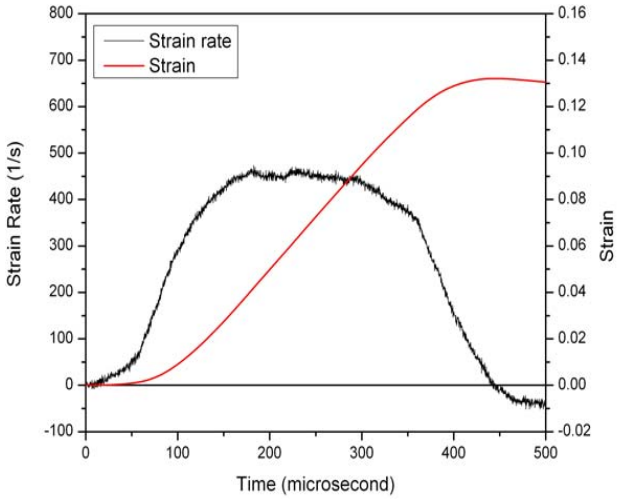

Figure 24. Strain-rate and strain histories for uniaxial experiment

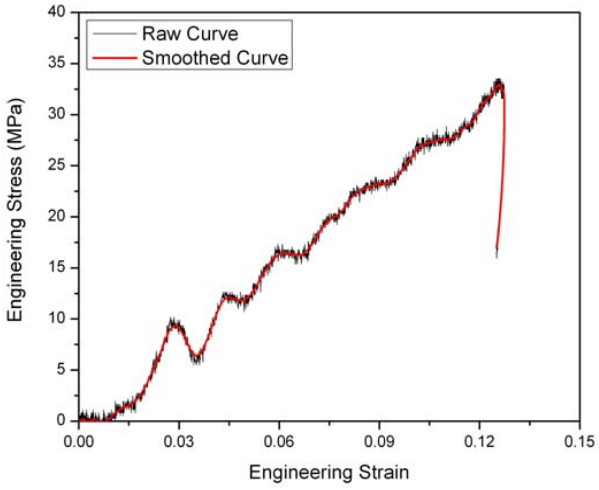

Figure 25. Dynamic stress-strain curves from a uniaxial experiment

To examine the repeatability of experiments and specimens, 23 experiments under an identical loading condition were conducted. Figure 26 summarizes all 23 stress-strain curves of the 1.50 g/cc dry sands confined with the PC tubes at the strain rate of ~470/s. Figure 27 presents the variation of stresses at the strains of 5% and 10% obtained from the 23 experiments. The results exhibit reasonable repeatability of the sand experiments.

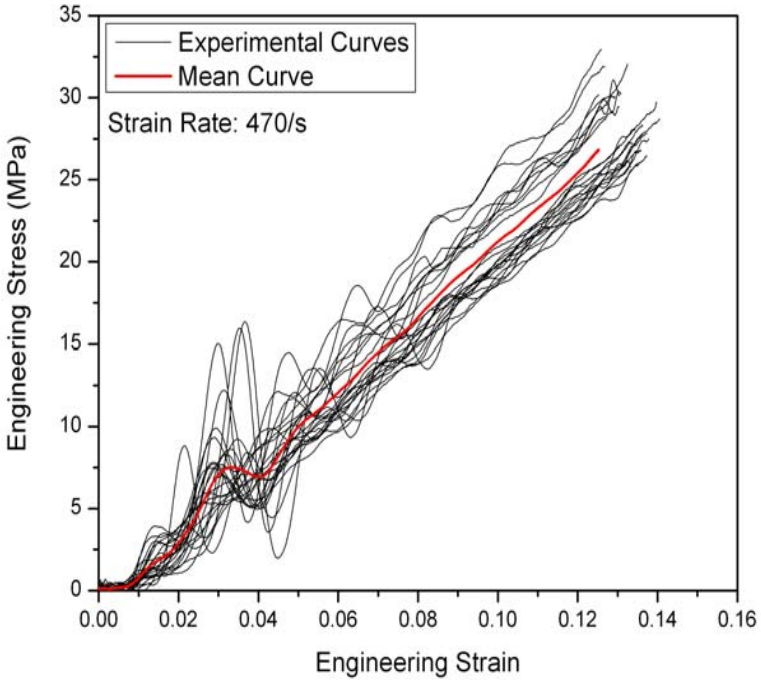

Figure 26. Stress-strain curves under identical loading conditions

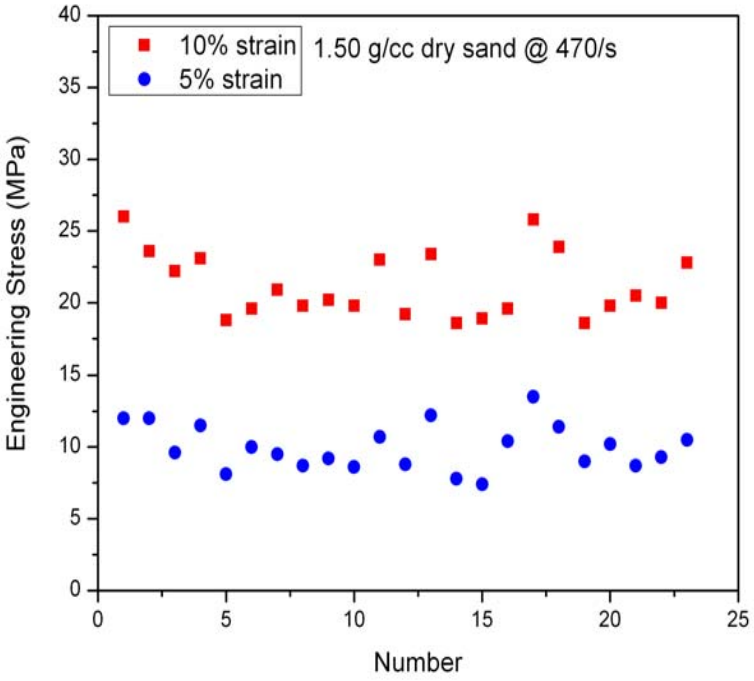

Figure 27. Distribution of stresses at 5% and 10% strains

Three dynamic strain-rate experiments (470/s, 900/s, and 1450/s) for the 1.50 g/cc dry sand were conducted to study strain-rate effect using similar procedures. At the strain rates of 470/s, various suites of dynamic experiments were also conducted: (1) on 1.62 g/cc dry sand to investigate density effect, (2) on wet sand with 7% weight water to examine moisture effect, (3) on 1.50 g/cc dry sand confined with the polyolefin heat shrink tubes, and (4) 4340 steel tubes to study the effect of lateral confinement.

Strain-Rate Effect

Since the sand specimens exhibit reasonable repeatability at the strain rate of 470/s, only five experiments were repeated at the higher strain rates of 900/s and 1450/s for the 1.50 g/cc dry sand. The stress-strain curves for these two strain-rates are shown in Figure 28 and Figure 29. The mean curves were used in addition to error bars to examine the strain-rate effects. Figure 30 presents the resulting dynamic compressive stress-strain curves, along with quasi-static results, which do not indicate significant strain rate effect of the 1.50 g/cc dry sand over this strain rate range.

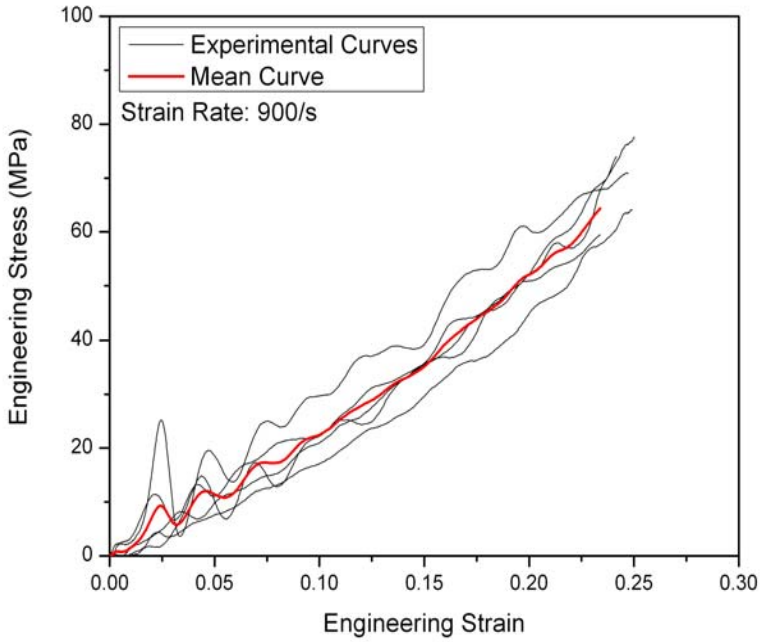

Figure 28. Stress-strain curves at the strain-rate of 900/s

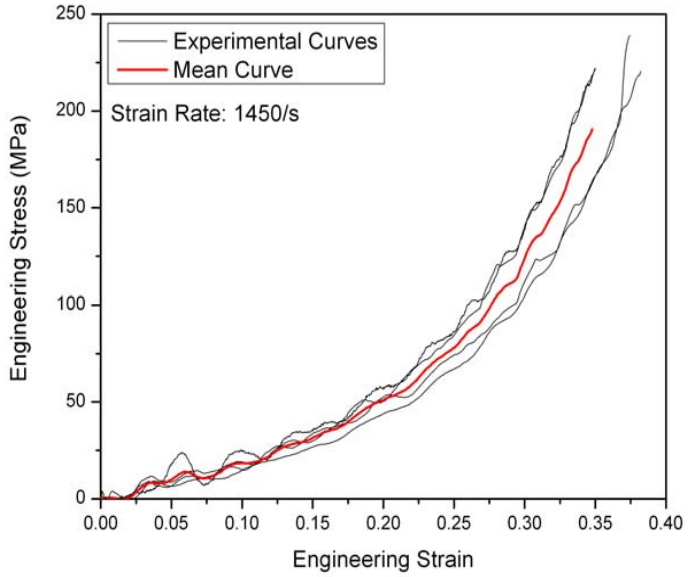

Figure 29. Stress-strain curves at the strain-rate of 1450/s

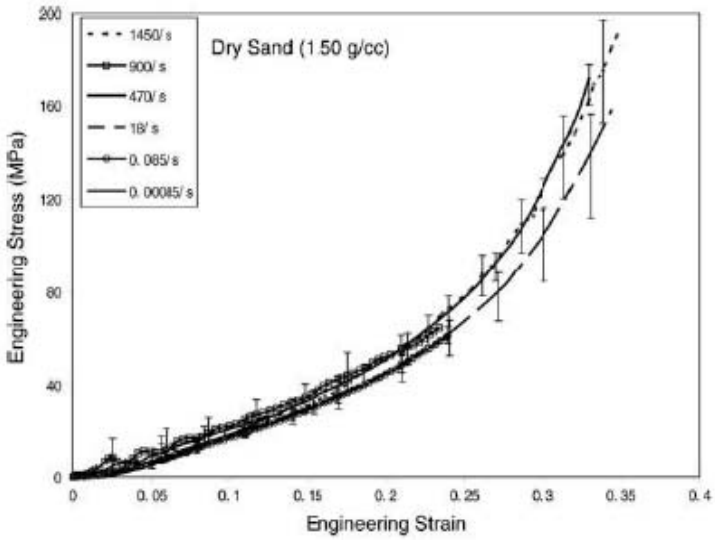

Figure 30. Stress-strain curves at six strain-rates

Density Effect

The dynamic compression stress-strain curves of 1.60 g/cc dry sand at the strain-rate of 520/s are shown in Figure 31. Five experiments were repeated and the mean curve was used to examine the density effect, as shown in Figure 32. The specimen stiffness increases significantly when the density increases from 1.50 to 1.62 g/cc, indicating strong density effects.

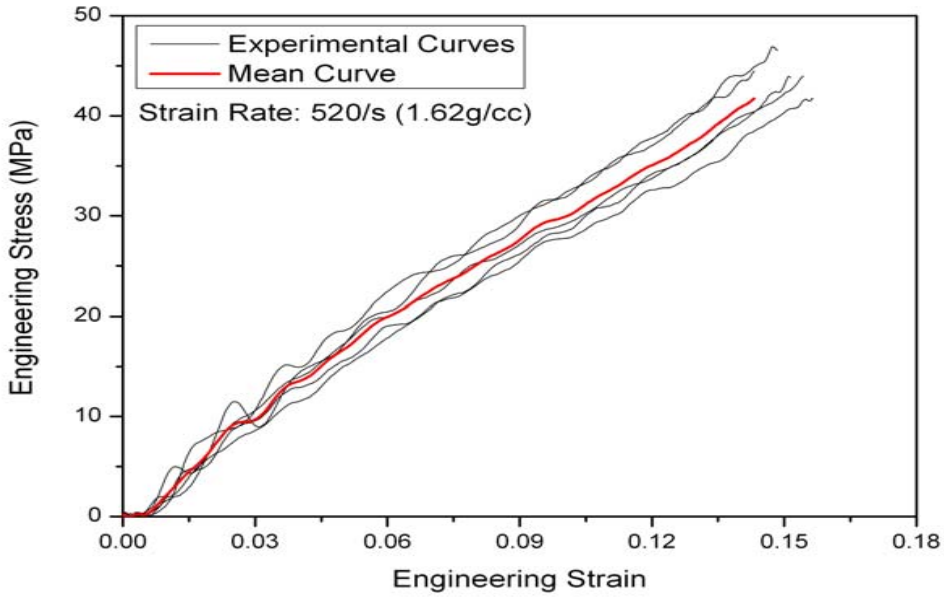

Figure 31. Stress-strain curves 1.62 g/cc dry sand at strain-rate of 520/s

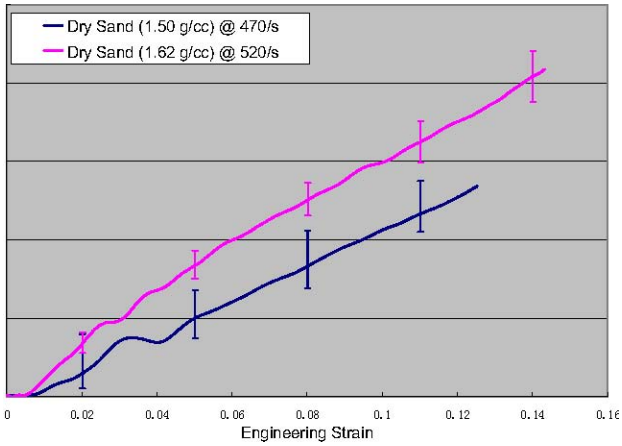

Figure 32. Comparison of stress-strain curves of 1.50 and 1.62 g/cc dry sand

Confinement Effect

Figure 33 and Figure 34 show the dynamic stress-strain curves of the 1.50 g/cc dry sand confined with the polyolefin heat shrink tube and the 4340 steel tube at similar strain rates, respectively. The stress-strain curves at similar strain rates under the three confinements are compared in Figure 35. The test results indicate that the sand specimens confined with the polyolefin heat shrink tube experience the lowest stresses while those confined with the steel tube are only slightly higher than those confined with the PC tube.

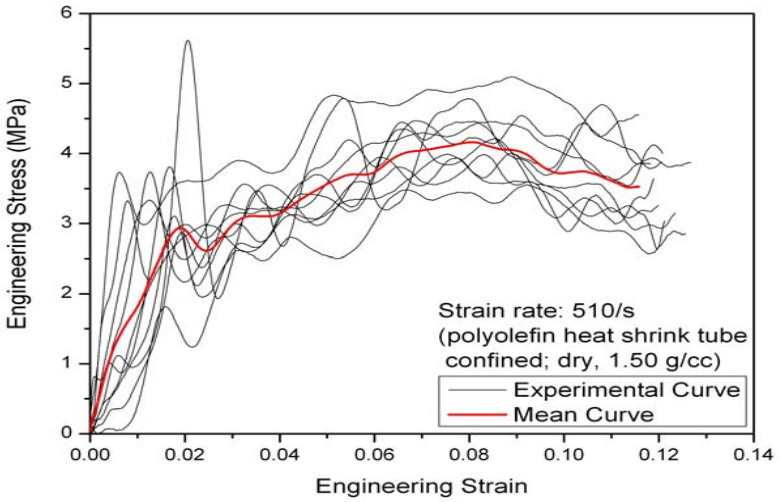

Figure 33. Stress-strain curves of 1.50 g/cc dry sand confined with polyolefin heat shrink tube

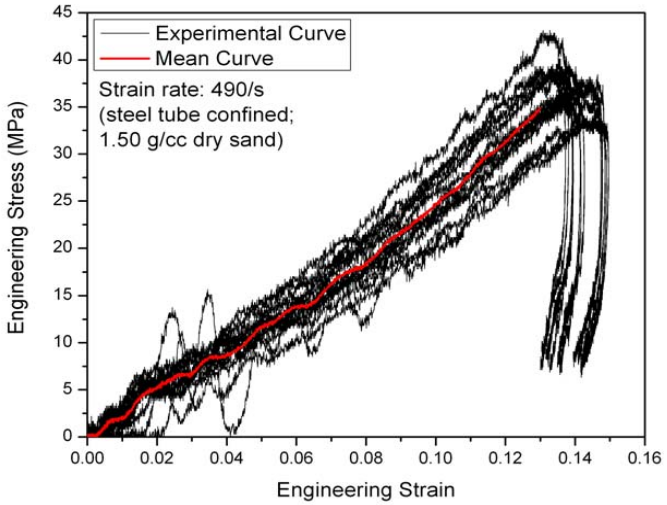

Figure 34. Stress-strain curves of 1.50 g/cc dry sand confined with steel tube

Figure 35. Comparison of stress-strain curves of 1.50 g/cc dry sand confined with steel, polycarbonate, and polyolefin tubes at similar strain rates

Dynamic experiments were also conducted on the polycarbonate at various strain rates. The 3.05-mm-thick circular PC tube was cut and separated into six equal parts as individual specimens, as shown in Figure 36 in order to achieve consistency with the PC tube material used in the sand confinement experiments. The pulse-shaped steel Kolsky bar was used for the dynamic characterization. Figure 37 shows the resultant stress-strain curves for the PC at the strain rates of 230, 440, and 1660/s.

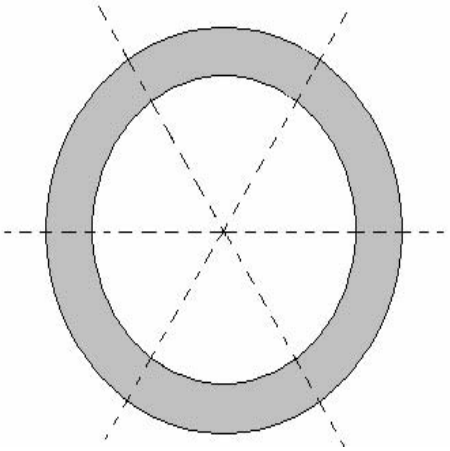

Figure 36. The PC specimens

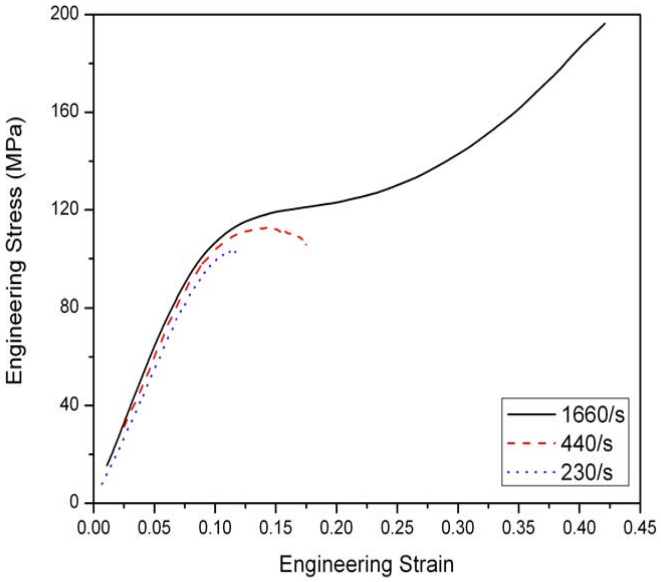

Figure 37. Dynamic stress-strain curves of the PC material

Moisture Effect

A total of 43 experiments were conducted with a strain-rate of approximately 400 s^1. All specimens were confined by a steel tube with moisture contents varying from 3% to 20% by weight. A minimum of five experiments were conducted at each moisture content, except at 5% moisture content where four experiments were conducted, to investigate the repeatability of the data. To illustrate the repeatability of experiments, all five stress-strain curves for 7% moisture

content are shown in Figure 38. A two sigma standard deviation was calculated using the five stress-strain curves in Figure 39 for percent strains of 1, 3, 5, 7, and 8. To limit confusion between errors for each moisture content, only those strains that showed error bars were chosen. The mean stress-strain curve with standard deviation for 7% moisture content is shown in Figure 39.

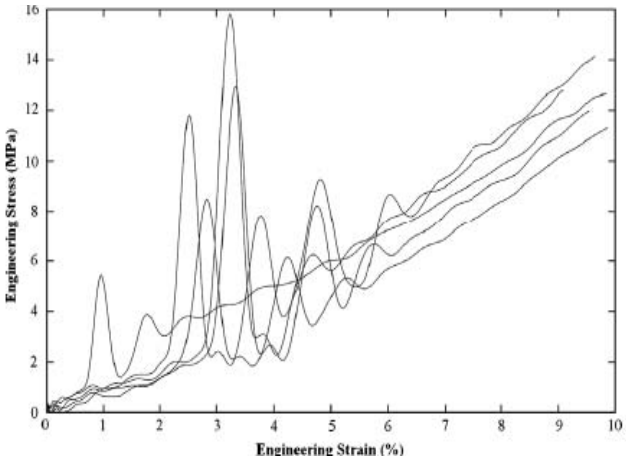

Figure 38. Dynamic stress-strain cures for 7% moisture content

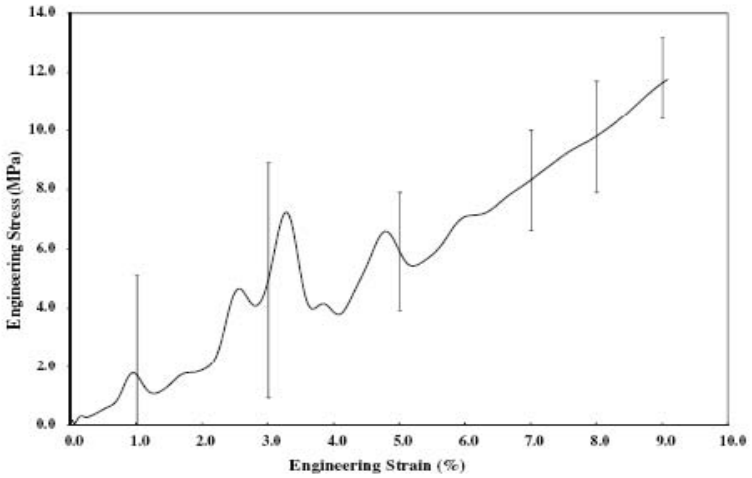

Figure 39. Mean stress–strain curve for 7% moisture content with standard deviation

The mean dry sand stress-strain response in Figure 40 was determined in a similar fashion. As shown in Figure 26 and Figure 27, the error ranges are very similar to that shown in Figure 39. The mean stress-strain curves for each moisture content show significant oscillations in stress between 2% to 4% strain. Oscillations are not evident for the dry sand mean stress-strain curve, but some of the 23 experiments conducted earlier (Figure 26) show similar oscillations. These oscillations are present for both dry and partially saturated conditions indicating that frictional effects, whether mechanical or inter-granular, may cause the oscillations, but no quantitative evidence exists at this time for this determination. The mean stress-strain relationships under steel confinement for this investigation are shown in Figure 40. For all experiments, the stress-strain curves are truncated at the maximum percent strain where both stress-equilibrium and constant strain-rate conditions are satisfied. The mean curves in Figure 40 represent the family of stress-strain curves at various moisture contents.

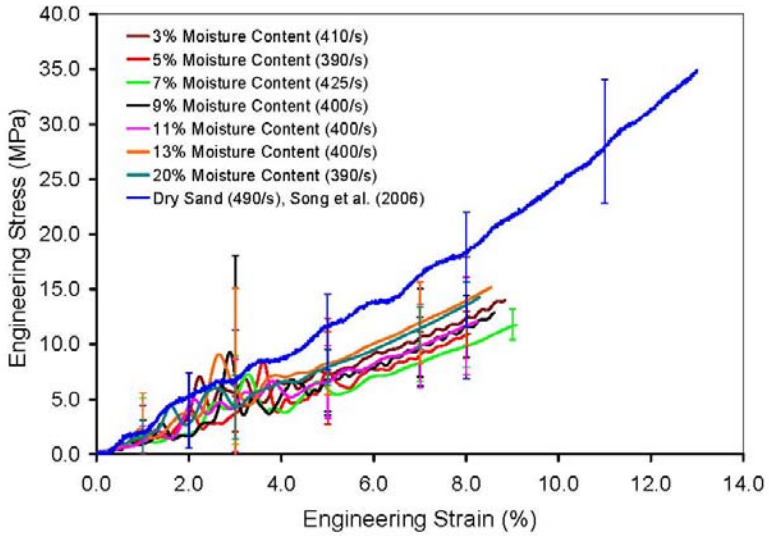

Figure 40. Mean stress-strain curves for Quickrete 1961 sand with steel confinement

The results in Figure 40 show that after the sand specimens are initially compacted, the oscillations in the stress-strain curves diminishes after a strain of 4%. The stress-strain behavior of the sand at all moisture contents is remarkably linear up to the strain of 8% to 9% when unloading initiates in the experiments with partially saturated sand. The dry sand results show the highest slope, corresponding to the stiffest behavior. As water is added progressively from 3% to 5% to 7% the stiffness decreases with increasing water content. As the water content is further increased, the sand specimen behavior stiffens. However, all the partially saturated sand is less stiff as compared to dry sand with specimens at 7% moisture content having half the stiffness of dry sand. The error associated with moisture contents between 3% to 11% have some overlap with the dry sand, whereas those associated with moisture contents between 13% and 20% have more overlap with the dry sand. Higher amounts of overlap exist between dry sand and 13% to 20% moisture contents due to higher quantities of water increasing the saturation of the specimen. When the saturation increases less air is present allowing water to be loaded and stiffening the response. Although these overlaps exist in the results, the trends of moisture effects can be clearly identified. Similar trends were also recorded in quasi-static experiments and will be discussed later.

6.1.2 Quasi-static Experiments

Quasi-static uniaxial strain tests have been accepted as well controlled experiments with well defined boundary conditions. In this section, results of quasi-static uniaxial strain experiments for dry and partially saturated sand conducted with the same boundary conditions and material are qualitatively compared to the results in this investigation.

A uniaxial strain test loads the specimen in the axial direction and constrains the specimen in the lateral direction with the radial loading and displacement recorded. All quasi-static uniaxial strain experiments for both dry and partially saturated sand were studied under comparable specimen conditions, using the experimental technique reported by Williams et al., 2006. The specimens were 50 mm in diameter and 110 mm in length having an aspect ratio of 2 compared to an aspect ratio of 0.49 for the specimens in this investigation. The specimens had an average dry density of 1.651 g/cm^3 for both the dry and partially saturated experiments. The dry sand

had a post-test moisture content of 0.5% with the partially saturated sand having a post-test moisture content of approximately 7.0%. All experiments were conducted at strain-rates of approximately 10^4 s^{-1} to 10^{-5} s^{-1}. The dry density is higher than the dry density in our studies, so only a qualitative verification of trends is appropriate. The uniaxial stress-strain response data for dry and partially saturated sand are shown in Figure 41. The associated error at each condition is represented by the differences between the two curves illustrating the repeatability of the data. The data shows that partially saturated sand is more compliant than dry sand which is consistent with the results obtained in this study. These results indicate that a small amount of water provides some lubrication between the particles making partially saturated sand more compliant than dry sand.

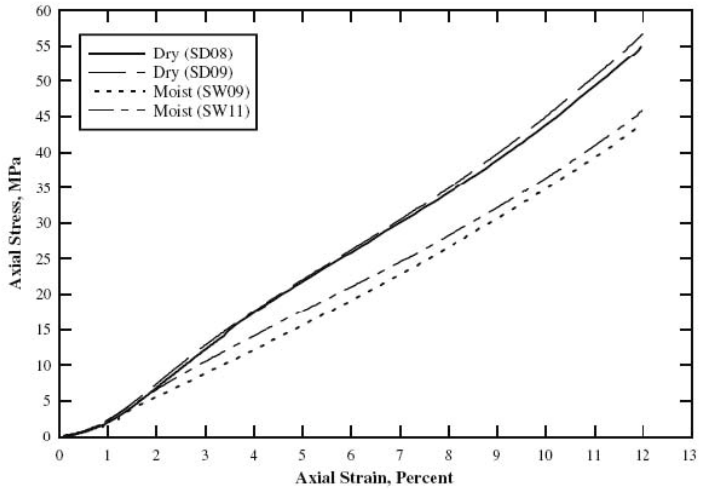

Figure 41. Quasi-static uniaxial stress-strain plot for dry and moisture sand

6.2 Triaxial Experiment

The specimens for triaxial experiments have a common dimension of 19.05 mm in diameter and 9.3 mm in thickness. The dry sand has a density of 1.50 g/cc. Figure 42 shows a typical set of LabVIEW records from the hydrostatic pressure phase of the experiment. The axial and radial strain signals were recorded along with the line pressure.

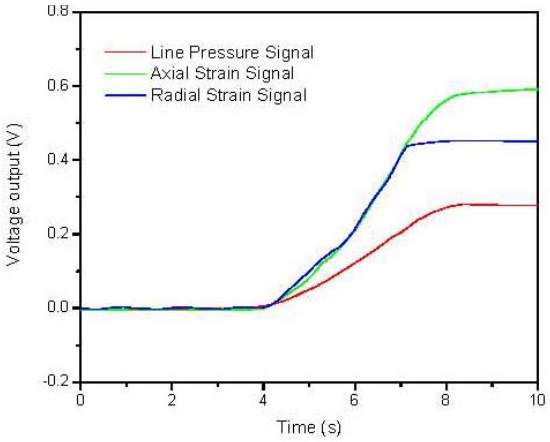

Figure 42. Typical set of axial, radial strain and line pressure signal from hydrostatic pressure phase

Figure 43 shows the typical oscilloscope records of incident, reflected, and transmitted pulses and radial strain and dynamic pressure signals. The shape of the incident pulse has been modified to ensure that the specimen deforms at a nearly constant strain rate under dynamic stress equilibrium. Figure 44 shows the dynamic stress equilibrium process in the specimen. The nearly overlapped stress histories at both ends of the specimen demonstrate that the stress in the specimen was uniform.

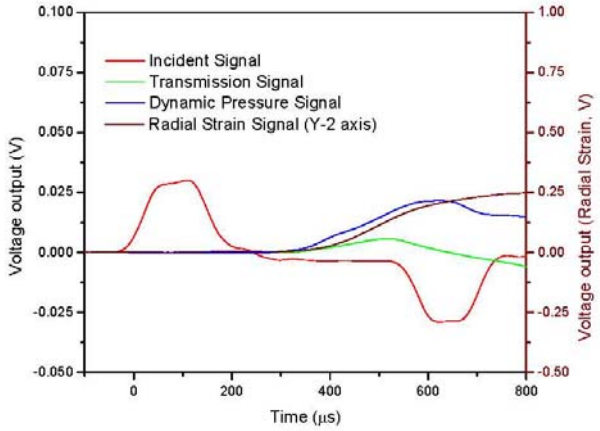

Figure 43. Typical incident, transmission signal along with dynamic pressure and radial strain signal

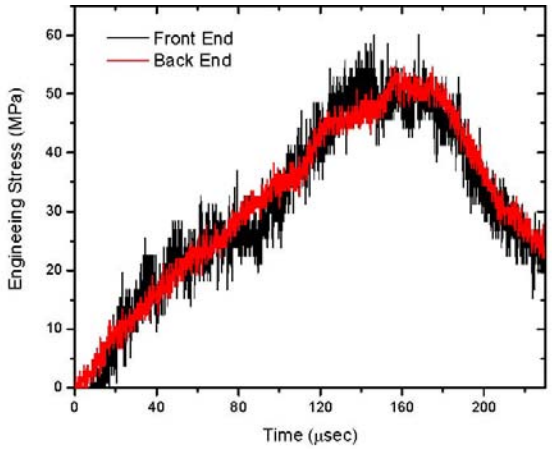

Figure 44. Dynamic Stress equilibrium process for triaxial experiment

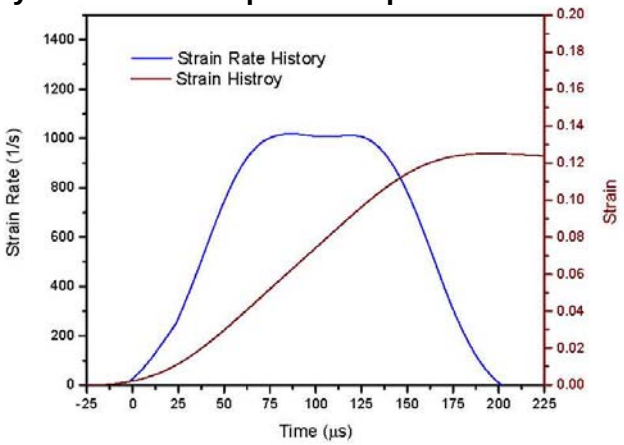

Figure 45. Typical strain rate and strain histories for triaxial experiment

Under the dynamic stress equilibrium, the reflected pulse represents the strain-rate history in specimen (Eq. (5)). Figure 45 shows the strain-rate and strain histories in the specimen. The strain rate is nearly constant (~ 100/s) from ~50 to 120 μs corresponding to the strains from 3% to 10%. Therefore, the specimen was deformed uniformly under dynamic stress equilibrium over most of the loading duration, indicating that the resultant stress-strain curve is valid and accurate.

The principal stress difference of the samples is plotted in Figure 456 and Figure 47 against the axial strain at 1000/s and 500/s strain rate respectively.

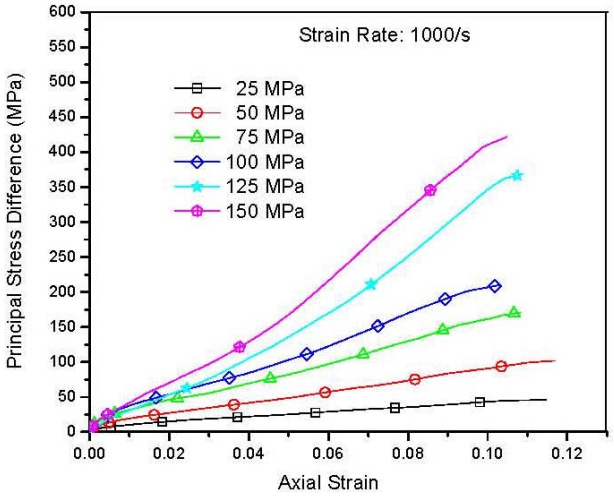

Figure 46. Principal stress difference-axial strain curves at 1000/s

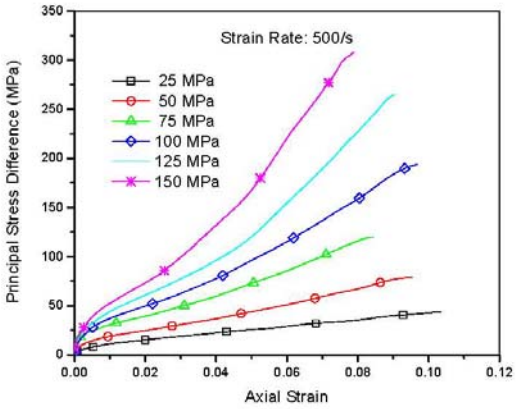

Figure 47. Principal stress difference-axial strain curves at 500/s

Triaxial experiments for the 7% moisture samples were conducted on the same fine grain sand specimens with a nominal diameter of 19 mm and nominal length of 9.3 mm. Two experiments were conducted at each confining pressure level. Samples were prepared with the similar technique as described for the dry sand triaxial experiments. Figure 47 shows the principal stress difference-axial strain curves at various confinement levels.

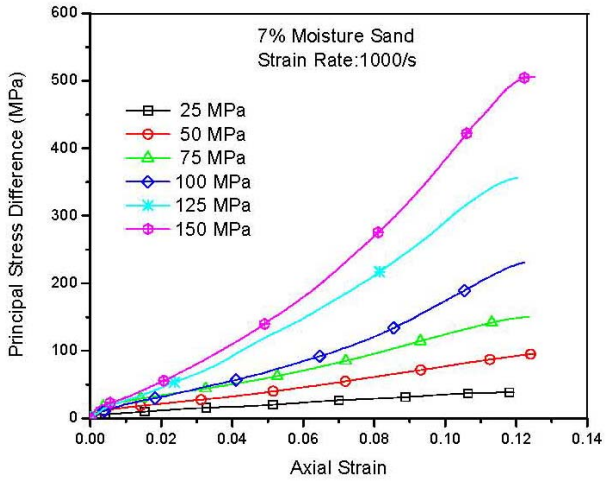

Figure 48. Principal stress difference-axial strain curves for 7% moisture sand at 1000/s strain-rate

6.2.1. Confinement Effect

Figure 46 and Figure 47 show the dynamic principal stress difference-axial strain curves of the 1.50 g/cc dry sand at various confining pressures at similar strain-rates, 1000s and 500, respectively. The curves at similar strain rates under the confining pressure indicate that the sand specimens are pressure sensitive. Higher pressure leads to stiffer response.

6.2.2 Strain Rate Effect

Five experiments were repeated at the strain rates of 500/s and 1000/s for the 1.50 g/cc dry sand. The principal stress difference-axial strain curves for these two strain rates are shown in Figure 46 and Figure 47. Mean principal stress difference at 7% axial strain was used in addition to error bars to examine the strain rate effect. The results shown in Figure 49 do not indicate significant strain rate effects of the 1.50 g/cc dry sand over this strain rate range.

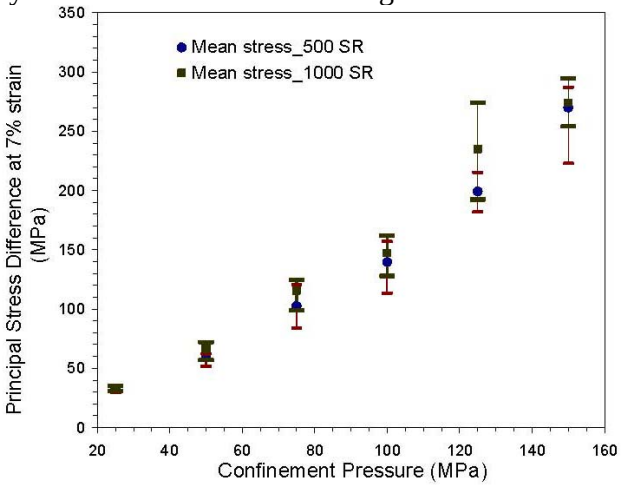

Figure 49. Principal stress difference at 7% axial strain level at various confining pressure

6.2.3 Moisture Effect

Figure 47 shows the principal stress difference-axial strain curves of the wet sand with 7% weight water at the strain rate of 1000/s. At the similar strain-rates, the stresses decreased significantly after 7% weight water was mixed in the specimen, as shown in Figure 50.

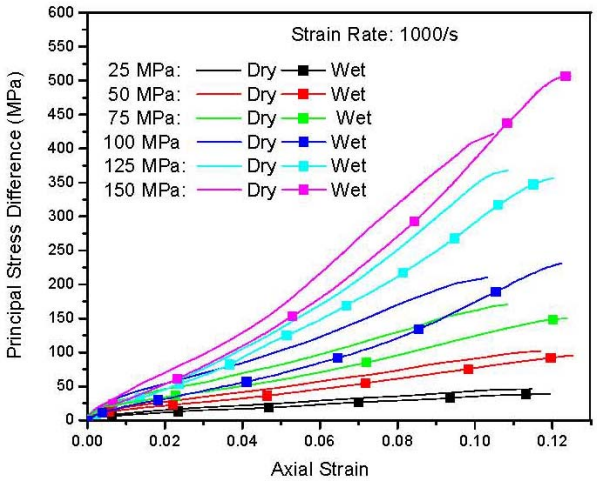

Figure 50. Moisture effect on the sand samples at 1000/s strain-rate

6.2.4 Particle Size Redistribution

We observed that after the hydrostatic pressure, the sand changed to a lighter color, as shown in Figure 21. After dynamic axial loading, the color further changed. This indicates that at least some of the sand particles have broken in the loading process. To quantitatively document the particle-size change, we conducted a grain size distribution analysis (sieve analysis, also commonly known as a "gradation test" on the sand before loading, after hydrostatic pressure, and after dynamic axial loading.

Five samples in each category (~ 20 g by weight) were screened using US standard sieves (Nos. 6-635) in an electromagnetic vibration sieve shaker. Sands were shaken at 2700 rpm for 15 minutes. After completion of the agitation of the sieves, the material retained in each sieve was weighed separately in a digital scale. For better accuracy the sieve with the sand was measured, rather than taking it out first.

Figure 51 shows the comparison between the steps of one triaxial experiment. It is seen that the sand particle size becomes smaller in each step. The curve for after hydrostatic phase is somewhat at the middle of the two extremes.

Figure 52 shows the grain size redistribution of the 1000/s strain-rate sand samples at various confinement levels after the dynamic impact. It is seen from these curves that the particle size gets smaller and smaller at each higher confinement level experiment. The comparative curve between two strain rates is shown in Figure 53. It is seen that the sand particle is redistributed to the similar level between both strain-rates.

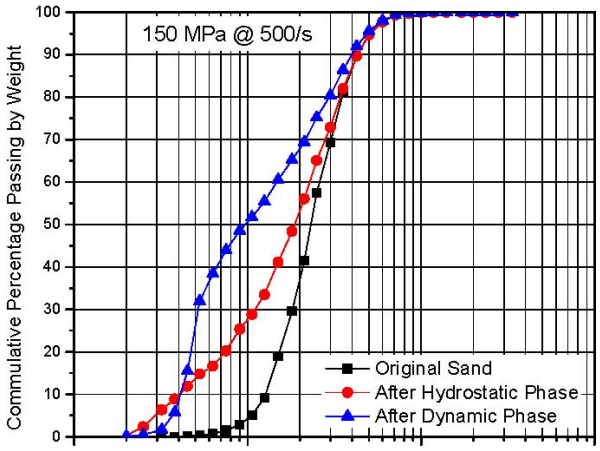

Figure 51. Sand grain size distribution at different stages of the experiment for samples of 150 MPa confinement and 500/s strain-rate

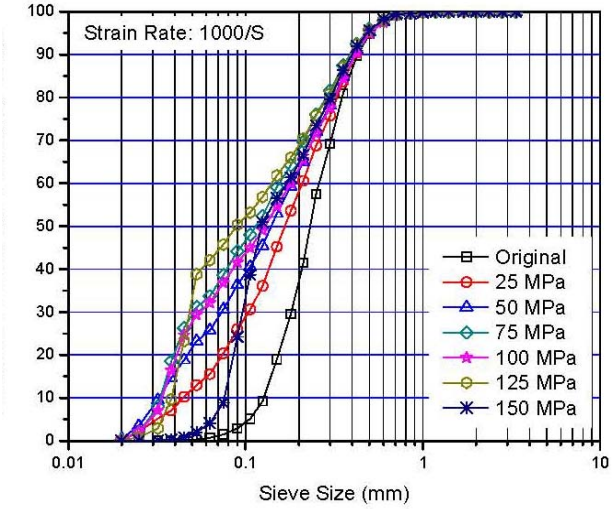

Figure 52. Sand grain size distribution for samples of 1000/s strain-rate

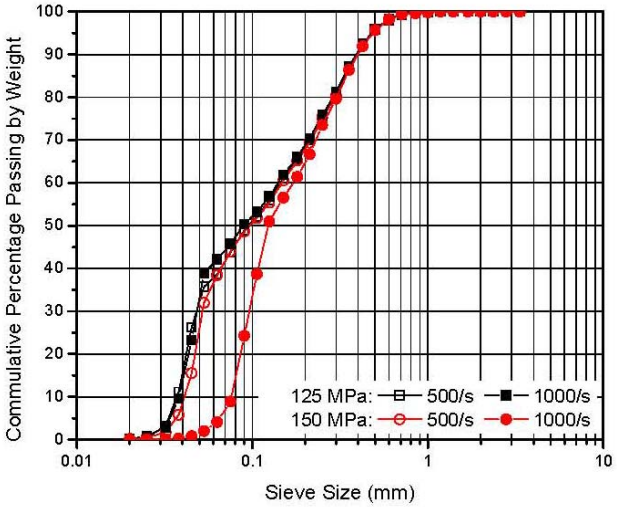

Figure 53. Comparison of sand grain size between two strain-rates

7 DISCUSSION

Dynamic uniaxial and triaxial mechanical response of sand from carefully designed experiments is not available in the literature. A comprehensive suite of modified Kolsky bar uniaxial and triaxial experiments were conducted to examine the effect of strain-rate, initial density, moisture content and lateral confinement on the stress-strain behavior of fine sand. These experiments give insight into the constitutive modeling of this material. The process of this experimental investigation provides many lessons learned to help guide future research in characterizing this category of geological materials.

1. Effect of strain-rates: The effect of strain-rates on both the uniaxial and triaxial compressive stress-strain response is not apparent over the strain-rate range studied. The strain-rate range investigated in this study is not sufficiently high to cover the deformation states in a granular target under penetration. There is a potential need to develop capabilities to conduct experiments for rates between Kolsky bar and plate impact experiments.

2. Effect of confinement: The confinement method used for the uniaxial experiment presented a mixed pressure/displacement boundary condition at the interface between the sand specimen and the confinement tube. This complicated boundary condition makes it difficult to examine the confinement effect. For example, the stress-strain behavior varied only slightly when the confinement was changed from a PC tube to a steel tube. However, the deformation behavior for these two cases was quite different. There was a significant lateral deformation in the PC-tube confinement case, involving an extensive shear deformation in the sand specimen. The steel tube, on the other hand, facilitated a nearly uniaxial strain deformation. In future experiments, more definitive lateral conditions need to be specified and achieved.

   In triaxial experiments, specimens were subjected to hydrostatic confinement which facilitates the examination of confinement effect. The confinement pressure has been varied systematically to examine its effect on the principal stress difference. As we have used heat shrink tube for the confinement, it provides little resistance on top of the hydraulic confinement. From the experiments it is evident that the principal stress difference depends on the confinement level. With application of higher confinement, the sand particles are crushed more, making the sample more packed.

3. Effect of moisture: The porosity of a given particulate material is dependent on the shape of the particles and the particle's size distribution. Dry sand can be considered as two-phase material: a solid corresponding to the sand skeleton and a gas associated with the pore air. If water or any other liquid is added then it is a three phase material (Hampton et al., 1966) unless it is fully saturated. In our investigation, the specimen consists of a sand skeleton and pores filled with air and water in an undrained state. If the specimen is strained sufficiently, all pore air or pore water will be removed from the volume if drained conditions prevail, but in undrained conditions pore air and pore water are displaced without leaving the volume. When all pore air is replaced by pore water the specimen is fully saturated and water is loaded causing the specimen to stiffen with little additional compression of the specimen.

The experiments conducted in the uniaxial experiment use steel confinement to contain the specimen. This condition preferentially allows axial strain to occur, since radial stress generated by the steel confinement will constrict lateral expansion. For uniaxial strain conditions, the volume fraction of air voids in the specimen is directly related to the percent strain required to remove the air voids. When the percent strain is equal to the maximum percent volume of air, it can be assumed that the specimen is fully saturated. The corresponding percent volume of air associated with each of the investigated moisture contents is tabulated in Table 2. In the dynamic experiment, the specimens were loaded to approximately 9% strain. With the maximum percent strains below the maximum percent volume of air voids, the effects of water are not dominant. The mean stress-strain curves in Figure 38 show no evidence of the material "locking up" where the specimen becomes completely saturated and water is loaded.

Table 2. Percent of air at varying moisture contents

% Moisture	Wet density (g/cc)	% Saturation	% Vol. of air
3	1.55	11	38.5
4	1.56	14	37.0
5	1.58	18	35.5
7	1.61	25	32.5
9	1.64	32	29.5
11	1.67	39	26.4
13	1.70	46	23.4
20	1.80	70	13.0

The results show that partially saturated sand is more compliant than dry sand. It is presumed that pore water acts as a lubricant at the inter-particle contact areas, decreasing the friction between the particles resulting in lower localized shear stresses. The trend present in the partially saturated sand is considered the results of the interactions between the moisture and sand particles in the specimen. At the lower moisture contents, the water between the particles lubricates the contact surfaces and enables the specimen to become more compliant. Subsequently, when the specimen becomes highly saturated, the pore water assumes the load acting to stiffen the specimen. The movement of sand particles, the lubrication of water, and increased hydrostaticity are all integrated phenomena that work together to influence the behavior of partially saturated sand.

A similar trend is also visible in the dynamic triaxial experiments. The principal stress difference in 7% moisture sand is lower than the corresponding dry sample. Wetting the sand sample makes it softer thereby the sample experiences more volumetric compaction than the dry counterpart.

4. Particle size redistribution: Sand samples were collected after each triaxial experiment for checking size redistribution. It is observed that a considerable amount of sand size redistribution occurred in each higher confinement level.

8. SUMMARY

We experimentally investigated the compressive mechanical response of fine sand. The strain-rate, initial density, stress state, and moisture level are systematically varied. A Kolsky bar was modified to apply dynamic compressive load on sand specimens with and without confinement. A controlled loading pulse generated by a pulse-shaping technique allows the specimen to acquire stress equilibrium and a constant strain-rate. Hydrostatic pressure chambers are integrated with the Kolsky bar to conduct dynamic triaxial experiments on the sand specimens. The results show that the compressive response of the fine sand is not sensitive to strain rate under the loading conditions in this study, but significantly dependent on the moisture content, initial density and lateral confinement. Partially saturated sand with moisture levels varying from 3% to 20% by weight is more compliant than dry sand, regardless of the moisture level. Similar trends were reported in the quasi-static regime for experiments conducted at comparable specimen conditions. The sand becomes stiffer as initial density and/or confinement pressure increases. A sieve analysis shows that the sand particle sizes become smaller after hydrostatic pressure, and furthermore, smaller after dynamic axial loading.

This page intentionally left blank

9. REFERENCES

ASTM, 2001. Annual Book of ASTM Standards – Soil and Rock, Section 4, Volume 04.08, Standard D2487, Conshohocken, PA.

ASTM D1921 - 06 Standard Test Methods for Particle Size (Sieve Analysis) of Plastic Materials.

Abrantes, A. E. and Yamamuro, J. A., "Experimental and Data Analysis Techniques Used for High Strain Rate Tests on Cohesionless Soil," Geotechnical Testing Journal, GTJODJ, 25 [2], 128-141 (2002).

Andersen, A. and Simsons, N. E., Norwegian Triaxial Equipment and Technique, proceedings, American Society of Civil Engineers Research Conference on Shear Strength of Cohesive Soils, Boulder CO, 1960, 695-709.

Bera, S.C. and Chattopadhyay, S., A modified Schering bridge for measurement of the dielectric parameters of a material and the capacitance of a capacitive transducer, Measurement 2003, 33, 3-7.

Bishop, A. W. and Henkel, D. J., The Measurement of Soil Properties in the Triaxial Test, 2nd ed. Edward Arnold, London, 1962.

Bishop, A. W. and Gibson, R. E., The influence of the Provisions for Boundary Drainage on Strength and Consolidation Characteristics of Soil Measured in Triaxial Test, in Laboratory Shear Testing of Soils, STP 361, American Society of Testing and Materials, Philadelphia, 1964, 435-451.

Bishop, A. W. and Wesley, L. D., A Hydraulic Triaxial Apparatus for Controlled Stress Path Testing, Geotechnique 1975, 25(4), 657-670.

Bragov, A. M., Grushevsky, G. M., Lomunov, A.K., 1996. Use of the Kolsky Method for Confined Tests of Soft Soils. Exp. Mech. 36(3), 237-242.

Bragov, A. M., Lomunov, A. K., Sergeichev, I. V., Tsembelis, K., Proud, W.G., 2008. Determination of physicomechanical properties of soft soils from medium to high strain rates. Int. J. Imp. Eng. 35, 967-976.

Bruno, D. and Randolph, M. F., "Dynamic and Static Load Testing of Model Piles Driven into Dense Sand," Journal of Geotechnical and Geoenvironmental Engineering, 125 [11], 988-998 (1999).

Charlie, W. A., Ross, C. A., and Pierce, S. J., "Split-Hopkinson Pressure Bar Testing of Unsaturated Sand," Geotechnical Testing Journal, 13 [6], 291-300 (1990).

Charlie, W. A., Dowden, N. A., Villano, E. J., Veyera, G. E. and Doehring, D. O., “Blast-Induced Stress Wave Propagation and Attenuation: Centrifuge Model Versus Prototype Test,” Geotechnical Testing Journal, GTJODJ, 28 [2], 1-10 (2005).

Chen, W., Lu, F., Frew, D. J., and Forrestal, M. J., "Dynamic Compression Testing of Soft Materials," Transaction of the ASME, Journal of Applied Mechanics, 69 [3], 214-223 (2002).

Dobry R., Ladd, R. S. Yokel, F. Y. Chung, R. M., and Powell, D., Prediction of Pore Water Pressure Buildup and Liquefaction of Sand During Earthquakes by the Cyclic Strain Method, National Bureau of Standards Building Science Series 138, Washington, DC, 1982, 154pp.

Duffy, J., Campbell, J. D., and Hawley, R. H., “On the Use of a Torsional Split Hopkinson Bar to Study Rate Effects in 1100-0 Aluminum,” ASME J. Appl. Mech., 37, 83-91, (1971).

Felice, C. W., Gaffney, E.S., Brown, J. A., Olsen, J. M., 1987a. Dynamic High Stress Experiments on Soil. Geotechnical Testing Journal GTJODJ 10(4), 192-202.

Felice, C. W., Brown, J. A., Gaffney, E. S., Olsen, J. M., 1987b. An Investigation into the High Strain-Rate Behavior of Compacted Sand Using the Split-Hopkinson Pressure Bar Technique. Proceedings of the 2nd Symposium on the Interaction of Non-Nuclear Munitions with Structures, Panama City Beach, FL**,** 391-396.

Follansbee, P. S., and Franz, C. E., “Wave Propagation in the Split Hopkinson Pressure Bar,” Trans. ASME, J. Eng. Mat. Technol., 105, 61-66 (1983).

Frew, D. J., Forrestal, M. J., and Chen, W., "Pulse-Shaping Techniques for Testing Brittle Materials with a Split Hopkinson Pressure Bar," Experimental Mechanics, 42 [1], 93-106 (2002).

Frew, D. J., Forrestal, M. J., and Chen, W., “Pulse Shaping Techniques for Testing High-Strength Steel with a Split Hopkinson Pressure Bar,” Experimental Mechanics, 45 [2], 186-195 (2005).

Gibson, R. E. and Henkel, D. J., Influence of Duration of Tests at Constant Rate of Strain on Measured Drained Strength, Geotechnique 1954, 4, 6-15.

Gray III, G. T., 1997. High-Strain-Rate Testing of Materials: The Split-Hopkinson Pressure Bar. LA-UR-97-4419, Los Alamos National Laboratory**,**. Santa Fe, NM.

Gray III, G. T., 2000. Classic Split-Hopkinson Pressure Bar Testing. Mechanical Testing and Evaluation, Metals Handbook, American Society for Metals, Materials Park, OH. 8, 462-476.

Gray III, G. T., Blumenthal, W. R., 2000. Split-Hopkinson Pressure Bar Testing of Soft Materials. Mechanical Testing and Evaluation, Metals Handbook, American Society for Metals, Materials Park, OH. 8, 488-496.

Germaine, J. T. and Ladd, C. C., Triaxial Testing of Saturated Cohesive Soils, Advanced Triaxial Testing of Soil and Rock, ASTM STP 977, Robert T. Donaghe, Ronald C. Chaney and Marshall.

L. Silver, Eds., American Society for Testing and Materials, Philadelphia, 1988, pp 421-459.

Hampton, D., Wetzel, R. A., 1966. Stress Wave Propagation in Confined Soils. AFWL-TR-66-56, Air Force Weapons Laboratory, Kirkland AFB, NM.

Henkel, D. J. and Gilbert, G. D., The Effect of the Rubber Membrane on the Measured Triaxial Compression Strength of Clay Samples, Geotechnique 1952, 3, 20-29.

Hopkinson, B., 1914. A Method of Measuring the Pressure Produced in the Detonation of High Explosives or by the Impact of Bullets. Philos. Trans. R. Soc. London, Ser. *A*, 213, pp. 437-456.

Hsieh, K. H., 1985, Techniques for Investigation of Sand Behavior under Cyclic Loading, Project Report OUR85-321p for Master of Science Degree, University of Massachusetts-Amherst.

Kitamura, R and Garuyama, M., Compression and Shear Deformation of Soil Under Wide-Ranging Confining pressure, Advanced Triaxial Testing of Soil and Rock, ASTM STP 977, Robert T. Donaghe, Ronald C. Chaney and Marshall L. Silver, Eds, American Society for Testing and Materials, Philadelphia, 1988, 501-511.

Kolsky, H., 1949. An Investigation of the Mechanical Properties of Materials at very High Rates of Loading. Proc.R. Soc. London, Ser. B 62, 676-700.

Lee, M. Y., Brannon, R. M. and Bronowski, D. R, 2004, Uniaxial and Triaxial Compression Tests of Silicon Carbide Ceramics under quasi-static loading conditions, Sandia Report SAND 20046005.

Li, H., Yang, H., Chang, C. and Sun, X., "Experimental Investigation on Compressive Strength of Frozen Soil Versus Strain Rate," Journal of Cold Regions Engineering, 15, 125-133 (2001).

Li, X. and Yang, W. L., "Effects of Vibration History on Modulus and Damping of Dry Sand," Journal of Geotechnical and Geoenvironmental Engineering, 124 [11], 1071-1081 (1998).

Li, X. S., Chan, Clarence K., and Shen. C. K., An Automated Triaxial Testing System, Advanced Triaxial Testing of Soil and Rock, ASTM STP 977, Robert T. Donaghe, Ronald C. Chaney

and Marshall L. Silver Eds., American Society for Testing and Materials, Philadelphia, 1988, 95-106.

Lindholm, U. S., 1964. Some Experiments with the Split Hopkinson Pressure Bar. J. Mech. Phys. Solids, 12, 317-335.

Macari, E. J. and Hoyos, L. R. Jr., 2001, Mechanical Behavior of an Unsaturated Soil Under Multi-Axial Stress State, Geotechnical Testing Journal 24 (1), 14-22.

Menzies, B. K., 1988, A Computer Controlled Hydraulic Triaxial Testing System, Advanced Triaxial Testing of Soil and Rock, ASTM STP 977, Robert T. Donaghe, Ronald C. Chaney and Marshall L. Silver, Eds, American Society for Testing and Materials, Philadelphia, 82-94.

Mitchell, J. K. and Soga, K., Fundamentals of Soil Behavior, 3rd Edition, John Wiley & Sons, Hoboken, NJ, 2005.

Nemat-Nasser, S., Isaacs, J. B. and Starrett, J. E., "Hopkinson Techniques for Dynamic Recovery Experiments," Proc. R. Soc. Lond., A, 435, 371-391 (1991).

Pestana, J. M. and Whittle, A. J., "Formulation of a Unified Constitutive Model for Clays and Sands," Int. J. Numer. Anal. Geomech., 23, 1215-1243 (1999).

Pestana, J. M., Whittle, A. J. and Salvati, L. A., "Evaluation of a Constitutive Model for Clays and Sands: Part I – Sand Behavior," Int. J. Numer. Anal. Geomech., 26, 1097-1121 (2002).

Peters, J.F., Determination of Undrained Shear Strength of Low Plasticity Clays, Advanced Triaxial Testing of Soil and Rock, ASTM STP 977, Robert T. Donaghe, Ronald C. Chaney and Marshall L. Silver, Eds, American Society for Testing and Materials, Philadelphia, 1988, 460474.

Pierce, S. J., 1989. High Intensity Compressive Stress Wave Propagation through Unsaturated Sands. Master Thesis, Colorado State University, Fort Collins, Co.

Pilla, S., Hamida, J. A. and Sullivan, N. S., Very high sensitivity ac capacitance bridge for the dielectric study of molecular solids at low temperature, Review of Scientific Instruments 1999, 70 (10), 4055-4058.

Ross, C. A., Nash, P. T., Friesenhahn, G. J., 1986. Pressure Waves in Soils Using a Split-Hopkinson Pressure Bar. ESL-TR-86-29, Air Force Engineering and Services Center, Engineering and Services Laboratory, Tyndall AFB, FL.

Veyera, G. E., 1994. Uniaxial Stress-Strain Behavior of Unsaturated Soils at High Strain Rates. WL-TR-93-3523, Wright Laboratory, Flight Dynamics Directorate, Tyndall AFB, FL.

Wang, Z., Hao, H. and Lu, Y., "A Three-Phase Soil Model for Simulating Stress Wave Propagation due to Blast Loading," Int. J. Numer. Anal. Geomech., 28, 33-56 (2004).

Williams, E. M., Akers, S. A., Reed, P. A., 2006. Laboratory Characterization of SAM-35 Concrete. ERDC/GSL TR-06-15, U.S. Army Engineering Research and Development Center, Geotechnical and Structures Laboratory, Vicksburg, MS.

This page intentionally left blank

APPENDIX A: BASIC RELATIONS TO THE TRIAXIAL TEST

Consider the deformation process of a specimen, placed in the confining chamber. During hydrostatic phase, same pressure is applied on the radial and longitudinal chamber, so the sample is in true hydrostatic state condition. Hence, the stress and strain tensor will be:

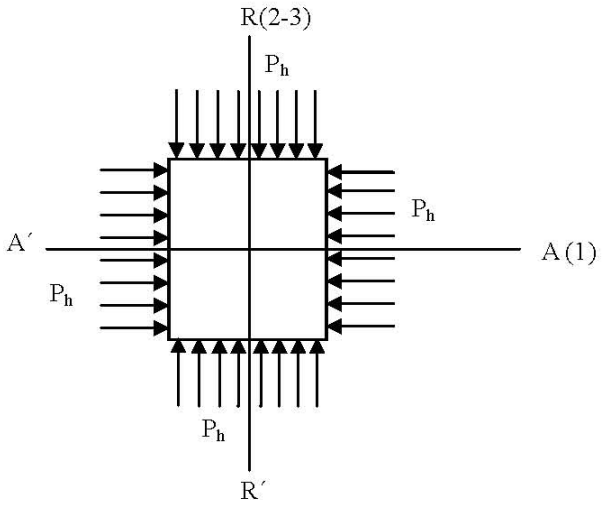

$$\sigma_1 = \sigma_2 = \sigma_3 = P_h \qquad \varepsilon_1 = \varepsilon_2 = \varepsilon_3 = \varepsilon_{ah} = \varepsilon_{rh} \qquad (8)$$

where $\sigma_{1\ldots3}$ are principal stresses, P_h is hydrostatic pressure, $\varepsilon_1 \ldots_3$ are principal strains, ε_{ah} is axial strain, and εrh radial strain.

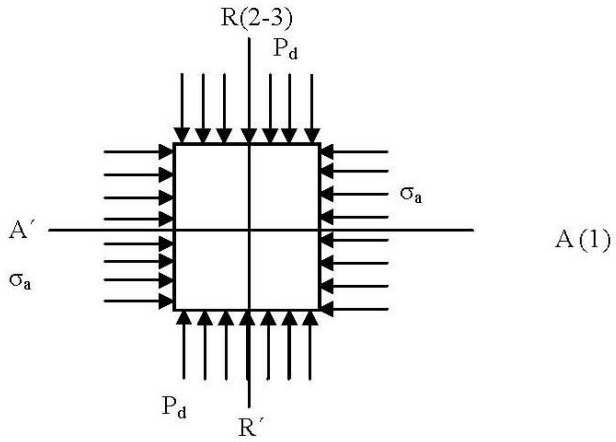

During the dynamic phase, an impact loading is applied axially in addition to hydrostatic pressure, P_h. The main components of the stress and strain tensors will be:

$$\sigma_1 = \sigma_a + P_h \qquad \sigma_2 = \sigma_3 = \sigma_r = P_h + P_d \qquad \varepsilon_1 = \varepsilon_a \qquad \varepsilon_2 = \varepsilon_3 = \varepsilon_r \quad (9)$$

where σ_a is axial stress and σ_r radial stress, while P_d is the dynamic pressure variation, ε_a is axial strain and ε_r radial strain.

The Maximum Tangential Stress, τ (resistance to shear) will occur at the planes inclined 45° to axis X. The Principal Stress Difference or the deviatoric stress, q (2xMaximum tangential stress, τ) on these planes will be:

$$q = 2\tau = \sigma_{ax} - \sigma_r \qquad (10)$$

The Mean Normal Stress, P in the specimen can be expressed in terms of the principal stresses as:

$$P = \frac{1}{3}(\sigma_a + 2\sigma_r) \qquad (11)$$

The volumetric strain will take the following form:

$$\varepsilon_v = \varepsilon_a + 2\varepsilon_r \qquad (12)$$

Thus having found σ_r, one can compute the Mean Normal Stress or the effective pressure P in the specimen. Expressions (11) and (12) as well as the uniaxial compression diagram, allow one to find the volumetric compressibility curve of the sample.

APPENDIX B: CALIBRATION CURVES FOR MEASURED PARAMETERS IN THE TRIAXIAL EXPERIMENT

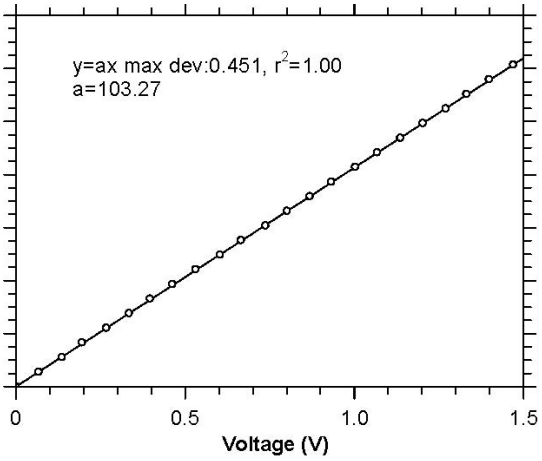

Figure B-1. Calibration for the line pressure gage

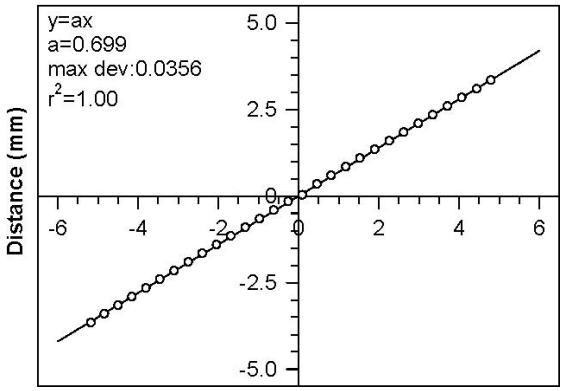

Figure B-2. Calibration curve for the LVDT for hydrostatic longitudinal strain measurement

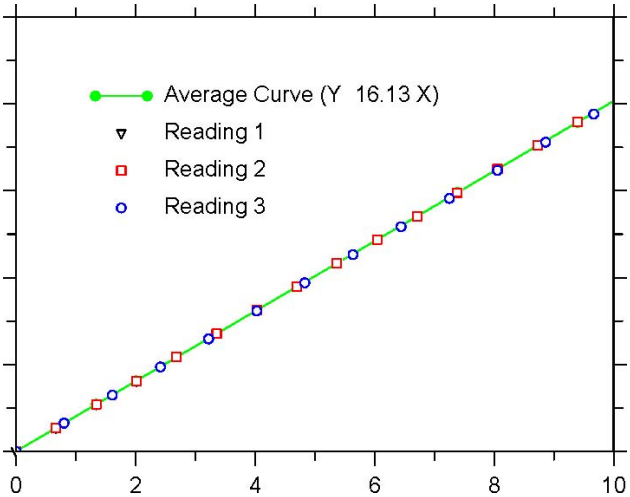

Figure B-3. Calibration curve for the Manganin pressure gage for dynamic pressure measurement

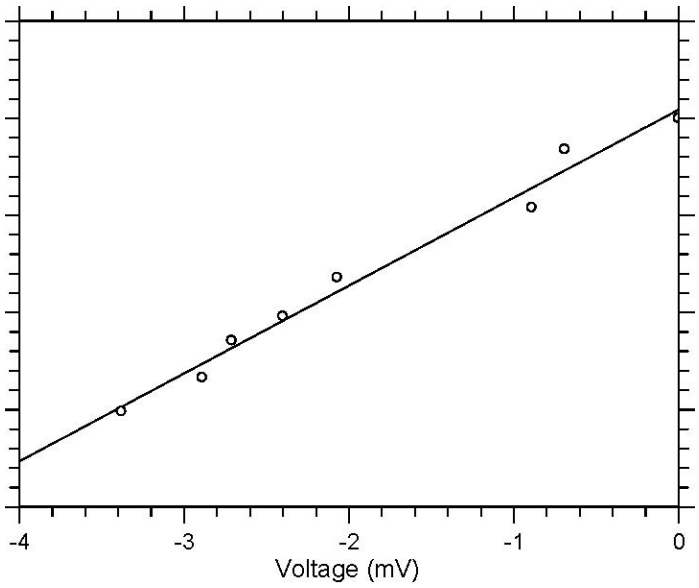

Figure B 4. Calibration curve for the hydrostatic and dynamic diametric strain measurement

APPENDIX C: DYNAMICS PRESSURE DISTRIBUTION

During the dynamic impact, the sample undergoes volume change therefore the pressure inside the test chamber varies with the loading. So it is necessary to measure the pressure distribution in the test chamber. We employed manganin pressure gages to record this variation of pressure. Three gages were placed radially at three different distances from the center of the sample to check the radial pressure variation. One at the front end of the sample and one at the middle of the sample were placed to record axial pressure distribution. Figure 1 shows the schematic of the manganin gage placement inside the test chamber. Figure 2 shows the actual photograph of the gage placement.

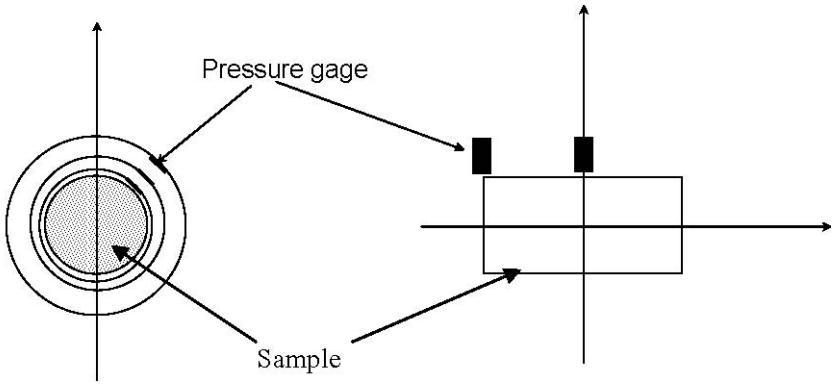

Figure C-1. Schematic of pressure gage placement with respect to the sample

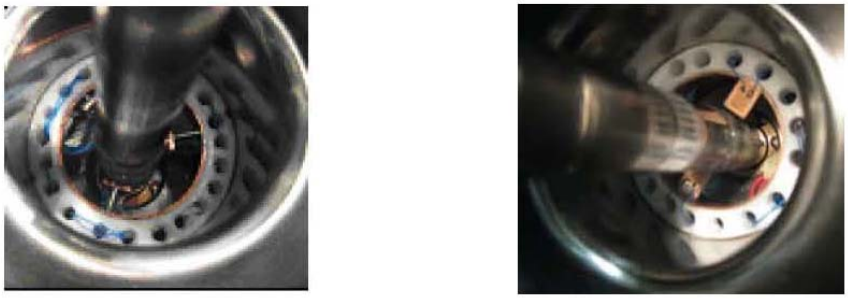

Figure C-2. Actual photograph of the pressure gage placement with respect to the sample

The reading from the pressure gages were recorded in the digital oscilloscope during the experiment. Figure 3 and 4 show the pressure distribution, radial and axial respectively. It is seen that the dynamic pressure variation in the test chamber during the impact are very close.

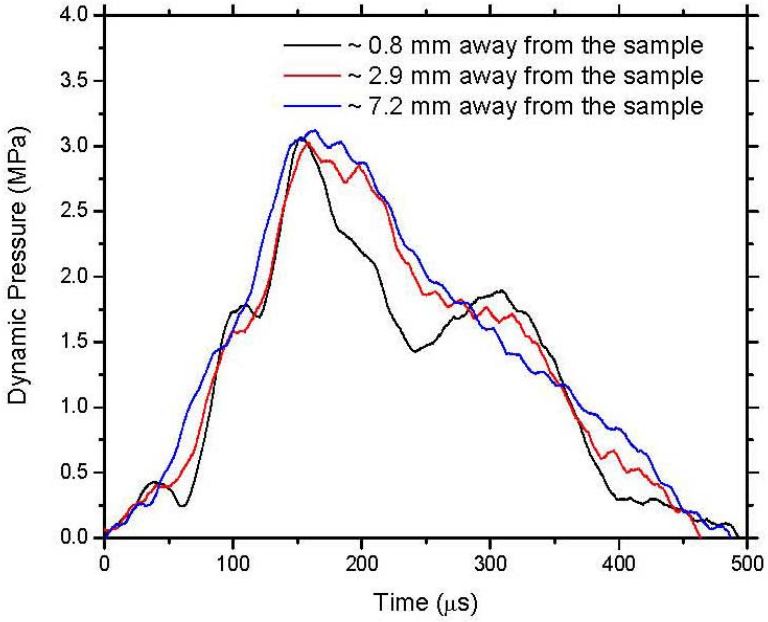

Figure C-3. Radial pressure distribution at 150 MPa confinement and 1000/s strain-rate

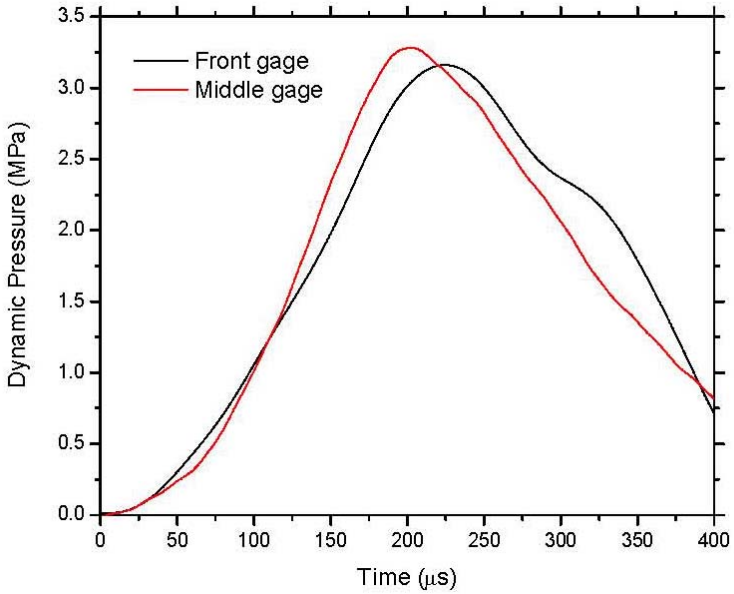

Figure C-4. Axial pressure distribution at 150 MPa confinement and 1000/s strain-rate

Electronic Distribution

External:

US Army Corp of Engineers, ERDC
Jeff Averett
Jeff.G.Averett@erdc.usace.army.mil

Donald Cargile
James.D.Cargile@erdc.usace.army.mil

Stephen Akers
Stephen.A.Akers@erdc.usace.army.mil

Andy Frank
Andreas.O.Frank@erdc.usace.army.mil

Defense Threat Reduction Agency, ASX
Richard Lewis
richard.lewis@dtra.mil

Office of the Secretary of Defense
Steve Deteresa
steve.deteresa@osd.mil

Defense Threat Reduction Agency, CX
Michael Giltrud
mike.giltrud@dtra.mil

Defense Threat Reduction Agency, CXT
Philip Randles
philip.randles@abq.dtra.mil

Eric Rinehart
eric.rinehart@abq.dtra.mil

Jeffery Thomas
jeffery.thomas@abq.dtra.mil

DTRIAC
Claude Fore
claude.fore_contractor@abq.dtra.mil

Army Research Laboratory, Aberdeen
Stephen Schrami
stephen@arl.army.mil

Purdue University
Wayne Chen
wchen@purdue.edu

Air Force Research Laboratory, Eglin
Mark Green
mark.green@eglin.af.mil

Robert Brown
robert.brown3@eglin.af.mil

Bradley Martin
bradley.martin@eglin.af.mil

Thomas Brantley
brantlet@eglin.af.mil

Martin Schmidt
martin.schmidt@eglin.af.mil

Bruce Patterson
bruce.patterson@eglin.af.mil

Brian Plunkett
brian.plunkett@eglin.af.mil

Defense Threat Reduction Agency, CXSS
Young Sohn
young.sohn@dtra.mil

Seung Lee
seung.lee@dtra.mil

Defense Threat Reduction Agency, CXWW
Danny Hayles
danny.haykes@dtra.mil

Robert Hastie
robert.hastie@dtra.mil

James A. Alley
James.Alley@dtra.mil

RD&E AMSRD-AMR-DS-WF
Thomas J. Gill
thomas.gill2@us.army.mil

Lawrence Livermore National Laboratory
Autoun Tarabay
antoun1@llnl.gov

Internal:

MS 1322	Stewart Silling, 1435
MS 0372	James M. Redmond, 1525
MS 0346	Joseph E. Bishop, 1525
MS 0380	Joseph Jung, 1542
MS 0751	Tom Pfeifle, 6735
MS0751	Laurence Costin, 6730
MS 1160	Damon Burnett, 5431
MS 1160	Douglas A. Dederman, 5431
MS 1160	James A. Dykes, 5431
MS 1160	John T. Foster, 5431
MS 1160	Eric W. Klamerus, 5431
MS 1160	John S. Ludwigsen, 5431
MS 1160	Vincent K. Luk, 5431
MS 1160	Paul Taylor, 5431
MS 1161	K. Terry Stalker, 5432
MS 1161	Dan M. Rondeau, 5430
MS 1162	Walter H. Rutledge, 5422
MS 1164	Paul C. Butler, 5435
MS 1164	William Guyton, 5400
MS 1164	Eric J. Schindwolf, 5430
MS 9042	Mike L. Chiesa, 8249
MS 9404	Bo Song, 8365
MS 0899	Technical Library, 9536 (electronic copy)